9-29-2017 3:00 PM

Assessment of Earthquake Site Amplification and Application of Passive Seismic Methods for Improved Site Classification in the Greater Vancouver Region, British Columbia

Frederick Andrew Jackson, *The University of Western Ontario*

Abstract

There is renewed interest to improve seismic microzonation mapping in Greater Vancouver, British Columbia (BC). We investigate local geology as the cause of observed variable ground shaking from the 2015 **M** 4.7 Vancouver Island earthquake. We observe high amplification at 4-6 Hz on thick sediment and the northern edge of the Fraser River delta, and disparities with current regional seismic microzonation mapping. Site amplification and shear-wave velocity (V_S) are assessed from the first borehole earthquake recordings in BC. We also perform ambient vibration analyses at 13 new locations in southwest BC to highlight suitability of passive seismic methods for improving regional microzonation. We obtain well-resolved V_S profiles from joint inversion of dispersion curves and horizontal to vertical spectral ratios. The corresponding National Building Code of Canada site classifications vary between D and C. This study is a notable contribution to public earthquake site assessments in the Greater Vancouver region.

Keywords

Co-authorship statement

The thesis is prepared in Integrated Article format and consists of the following two papers that are either published or submitted to peer-reviewed journals.

Chapter 2: Jackson, F., Molnar, S., Ghofrani, H., Atkinson, G.M., Cassidy, J.F., Assatourians, K. Ground Motions of the December 2015 **M** 4.7 Vancouver Island Earthquake: Attenuation and Site Response. *Bulletin of the Seismological Society of America*, accepted.

Strong-motion recordings were obtained by my supervisor. I generated my own Python codes (ObsPy) to perform all processing of strong-motion earthquake recordings (e.g., filtering, Fourier transformation, spectral ratios) and their interpretation with regards to previous studies and microzonation mapping. My work was combined with attenuation analyses of broad-band seismograph recordings accomplished by Dr. Hadi Ghofrani to comprise the full article and reviewed by our co-authors. Only my strong-motion analyses (second half of article) appear here in this thesis.

Chapter 3: Jackson, F., Molnar, S., Ventura, CE. Application of passive seismic methods at 13 school sites to improve earthquake site assessment in the Greater Vancouver region, British Columbia, Canada. This paper will be submitted to the Canadian Geotechnical Journal or the Canadian Journal of Civil Engineering.

Passive seismic recordings were collected and provided by my supervisor. I performed all the ambient vibration analyses and inversions for each site using Geopsy software. I generated a Matlab script to efficiently display Geopsy results and produce figures for publication. I obtained previous studies with independent datasets to compare and interpret my results.

The thesis and integrated articles were completed under the supervision of Dr. Sheri Molnar. Dr. Molnar provided on-going guidance, suggestions, and improvements to the manuscripts and assisted with manuscript revisions.

Acknowledgments

I'm enormously grateful to my supervisor Sheri. She provided me with the opportunity to study my MSc at Western, and throughout my years of study has been incredibly supportive and open to any questions I had.

I'd also like to thank all the coauthors of my BSSA paper: Hadi Ghofrani, Gail M. Atkinson, Karen Assatourians, and John Cassidy. Their kind guidance during my project and their contributions to the published paper are much appreciated.

Finally, I must express my profound thanks to my friends and family for all their support. This accomplishment would not have been possible without them.

Table of Contents

List of Tables

List of Figures

List of Appendices

List of Abbreviations

1D	One-dimensional
2D	Two-dimensional
3D	Three-dimensional
BC	British Columbia
BC MoTI	BC Ministry of Transportation and Infrastructure
BCSIMS	BC Smart Infrastructure Monitoring System
CHBDC	Canadian Highway and Bridge Design Code
CSZ	Cascadia Subduction Zone
EHVSR	Earthquake Horizontal-to-Vertical spectral ratio
FK	Frequency Wavenumber
GMPE	Ground Motion prediction Equation
HRFK	High Resolution Frequency Wavenumber method
HVSR	Horizontal-to-Vertical spectral ratio
IA	Internet accelerometer
MASW	Multichannel Analysis of Surface Waves
MHVSR	Microtremor Horizontal-to-Vertical spectral ratio
MSPAC	Modified Spatial Auto Correlation
NBCC	National Building Code of Canada
NEHRP	National Earthquake Hazards Reduction Program
NRC	Natural Resources Canada
PGA	Peak ground acceleration (%g)
SASW	Spectral Analysis of Surface Waves
SH	Transversely-polarised shear wave
SV	Vertically-polarised shear wave
SPAC	Spatial Auto Correlation method

List of Symbols

A	Impedance amplification
f_0	Fundamental peak frequency (Hz)
g	Acceleration due to gravity (m/s^2)
f_{peak}	Response peak frequency (Hz)
h	Layer thickness (m)
k_{max}	Aliasing Limit
k_{min}	Resolution Limit
M	Moment Magnitude
n	Normal mode number
R_{hypo}	Hypocentral distance (km)
V_S	Shear-wave velocity (m/s)
V_{S30}	Time-averaged shear-wave velocity of the upper 30 meters (m/s)
V_{Save}	Time-averaged shear-wave velocity of the soil layer (m/s)
ρ	Density (kg/m^3)

Chapter 1

1. Introduction

1.1. Seismic risk in British Columbia

Greater Vancouver is the largest metropolitan area in British Columbia (BC), and is the highest earthquake risk city in Canada due to significant exposure to high hazard. As the third largest city in Canada, it encompasses a population of 2.5 million, as well as key infrastructure including Canada's second busiest airport, the fourth largest tonnage port in North America, and 22 major bridge and tunnel crossings. Greater Victoria, the provincial capital, is located at the southern tip of Vancouver Island and includes a population of 345,000; the island relies on submarine electrical transmission cables, and ferry terminals for 95% of its food supply, from the BC mainland. A report commissioned by the Insurance Bureau of Canada (AIR Worldwide, 2013) estimates that a moment magnitude (**M**) 9.0 earthquake in BC would cause $62 billion in direct damages, and an additional $12.7 billion in indirect impact (e.g. supply chain interruption, infrastructure damage).

60% of Canada's earthquakes occur along BC's coast (Natural Resources Canada, 2016). The high seismic hazard in this region arises from the 1000 km long Cascadia Subduction Zone (CSZ), which stretches from Vancouver Island to northern California and marks the subduction of the Juan de Fuca plate under the North American plate (Figure 1.1). This zone is bounded by two transform faults: the Queen Charlotte Fault to the north, and the San Andreas Fault to the south. Southwest BC is located at the northern end of the CSZ (see Figure 1.1). Southwest BC is a region of complex deformation above a bend in the subducting plate. Crustal structure here in the continental margin is composed of accreted metamorphic and igneous terranes with various mapped faults at surface and at depth (Balfour, 2011). As is common with subduction zones, the CSZ is associated with a chain of andesitic volcanoes that extend from northern California to southern BC (Clague, 1997).
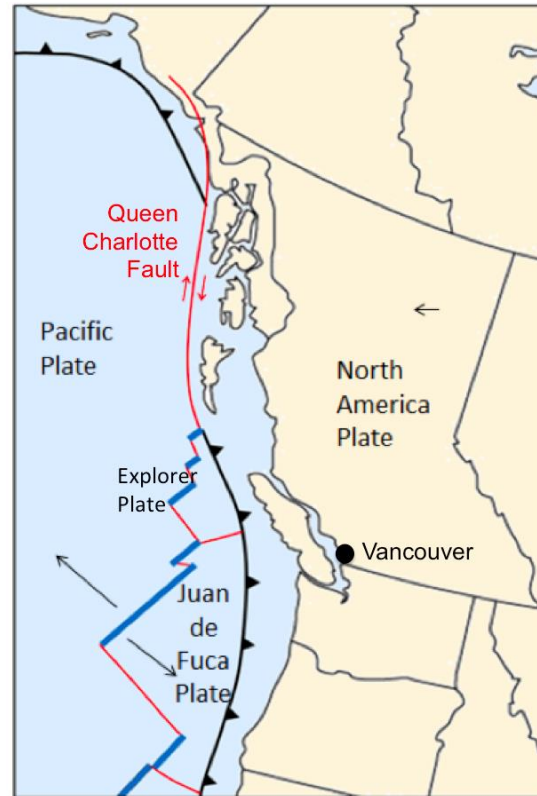
Figure 1.1. Tectonic setting of the northern Cascadia Subduction Zone. Arrows show relative plate motions. (Modified from Earle, 2016).

Southwest BC is one of the most seismically active regions in Canada: more than 100 offshore earthquakes of magnitude 5 or greater have occurred in the last 70 years (CREW, 2011). The complex tectonic setting gives rise to three types of earthquakes: those originating at the subduction interface (interplate), inside the subducting plate (inslab/intraplate), and at shallow faults in the crust (crustal). The largest instrumentally recorded earthquake in Canada was the 1949 **M** 8.1 crustal event near Haida Gwaii (Natural Resources Canada, 2016), which originated from the strike-slip movement of the Queen Charlotte Fault. The magnitude of inslab events is usually lower than **M** 7, but due to their high rate of occurrence, make the largest contribution to seismic hazard in the region (Bent & Greene, 2012), particularly short-period ground shaking. Most recently, motions of the 2015 **M** 4.7 Vancouver Island inslab earthquake demonstrated high stress (Brune source model) but lower shaking levels than expected (GMPEs are not well tuned to this low magnitude level; Jackson et al., 2017). In addition, there is significant

evidence that the Juan de Fuca and North America plates are currently locked together (Clague, 1997), allowing the possibility of a sudden release of the accumulating strain resulting in a rare subduction "megathrust" earthquake, like the 1700 Cascadia megathrust earthquake, estimated as **M** 8.7-9.2 (Satake et al., 2003). However these mega-thrust events occur on average only once every 500 years.

Because of the significant seismic hazard in southwest BC, it is vital to predict future earthquake ground motions as accurately as possible. The accuracy of seismic hazard estimates affects building codes and earthquake risk and loss estimations. Effective risk assessment affects the government's ability to save lives and money by identifying at risk regions and structures and to guide decisions on resource allocation.

1.2.   Project Aims

In response to renewed interest to improve seismic microzonation mapping in Greater Vancouver, we aim to first qualify the accuracy of current microzonation mapping in the region, and secondly test the suitability of non-invasive seismic techniques to address these issues by site-specific V_S profiling. Specifically we aim to determine important parameters that govern site response, e.g., V_S profile(s), fundamental peak frequencies, and depths of significant impedance contrasts.

The overall impact of this study is to add to the database of knowledge on seismic velocities in Metropolitan Vancouver as a continuation of passive-seismic site characterization case studies in BC (Molnar et al., 2010; Molnar et al., 2013; Molnar et al., 2014) which serve as the basis for a 5-year seismic microzonation effort in the region. Accurate V_S mapping will improve the hazard mapping in the region and thus the ground motion prediction and risk estimation.

1.3.   Seismological theory

Energy released by an earthquake propagates as two basic types: body waves which travel directly from the earthquake focus through the Earth's interior, and surface waves generated by the interaction of body waves at the Earth's surface, which travel laterally

along the free boundary of the surface. Body waves consist of compressional or primary (P) waves, which propagate longitudinally along the direction of motion, and shear or secondary (S) waves, which propagate radially to the direction of motion. Shear waves can also be polarised into either perpendicular plane by geological interaction into either SH (shear-horizontal) or SV (shear-vertical). P-waves travel fastest with low amplitude, and S-waves travel slower with higher amplitude due to the conservation of energy.

Surface waves consist of two types: Love waves consisting of a horizontally polarised (SH) S-wave trapped in the upper layers of the surface, and Rayleigh waves generated by the interference between a lateral P-wave and an SV-wave. Surface waves travel slower than body waves and arrive last, but with considerably higher amplitude and duration, meaning that they commonly cause the most destruction in an earthquake event.

Commonly the horizontal shear motions are the most significant component of seismic load in ordinary buildings (Panza et al. 2004), and therefore the most damaging aspect of earthquake shaking. Because of this, high amplitude Love waves tend to be the most damaging wave, as well as standard S-waves propagating close to the earthquake source where their amplitudes have not yet decayed by geometric attenuation. For moderate earthquakes, the peak ground acceleration (PGA) is the main control of observed damage, however in severe earthquakes damage is mainly controlled by the peak ground velocity (Worden & Wald, 2016).

1.4. Site Effects

In many historical and recent earthquakes local geology and soil conditions have notably altered the amplitude, frequency content and duration of ground motion, resulting in significant variation across small regions. A notable case study for the contribution of site effects is the 1985 **M** 8.0 Mexico City earthquake, where the city experienced catastrophic damage on soft lake bed deposits from the megathrust event over 350 km away (Seed et al., 1988). This phenomenon is known as site effects, and includes amplification and resonance from the one-dimensional (1D) soil column as well as from two- (2D) and three-dimensional (3D) basins and topography. Observed amplification is

also affected by complex dynamic properties of soil (damping, plasticity, liquefaction) however these effects are not further considered in this thesis. Site effects can often be adequately described by 1D models, although in areas of strong lateral variations a spatial understanding of site effects is required (Sánchez-Sesma, 1987). Proper characterization of site conditions is a major component of seismic hazard analysis and required for accurate ground motion prediction.

There are two major site effect factors that amplify ground motion as seismic waves propagate through a 1D column of soil (profile): shear wave velocity (V_S), and impedance contrast thickness. Firstly, V_S of a material is directly related to the stiffness, and seismic waves travel slower and with higher amplitude through soft sediments compared to stiff material due to the conservation of energy. As previously stated, the horizontal shear motions are commonly the most significant component of seismic load in ordinary buildings (Panza et al. 2004), i.e. the SH component in both S-wave and Love wave propagation. Therefore V_S is a major control of earthquake damage.

Because shear waves refract towards the vertical as they propagate through less stiff layers towards surface, and because the direction of particle motion is perpendicular to propagation, amplification is observed in the horizontal component of motion. For a single soil layer (subscript 1) over an elastic half-space (subscript 2), the theoretical 1D impedance amplification (A) is:

$$A = \sqrt{\frac{\rho_2 V_{S2}}{\rho_1 V_{S1}}}, \tag{1.1}$$

where ρ is density.

Secondly, when a site consists of soft surficial material, its thickness and the depth to a major impedance contrast such as stiff bedrock has a large effect on amplification. The resonance amplification is equal to Equation 1.1 squared, which occurs at the following frequencies:

$$f = (2n + 1)\left(\frac{V_{Save}}{4h}\right), \tag{1.2}$$

where *n* is the normal mode number (defined by the number of half-sinusoidal waves in the vibration), V_{Save} is the average velocity of the soil layer, and *h* is thickness. The described 1D site amplification defines a SH-wave transfer function or amplification frequency spectrum. Soils behave nonlinearly when earthquake shaking is strong, i.e., ~10 %g, where g is the acceleration due to gravity. 1D earthquake site response includes the nonlinear behaviour of the soil itself when shaken by dynamic earthquake shaking. Prediction or modelling of 1D earthquake site response includes V_S and ρ (small-strain shear modulus; $G_{max} = \rho V_S^2$) as well as shear modulus reduction and damping curves established for various soil types (e.g., Seed & Idriss, 1970).

Site characterization includes field and laboratory methods to measure properties (i.e., V_S and ρ) of the subsurface geologic material at the site to describe and ultimately predict earthquake site effects. Field techniques can be geotechnical (standard penetration tests, pressure meter tests, seismic cone penetration tests, etc.) or geophysical (active- or passive-source surface wave methods). Geophysical (seismic) field techniques are much faster and non invasive, and are better suited for a large-scale site characterization project. Mapping large-scale seismic hazard variation due to site conditions is known as seismic microzonation mapping, and typically includes amplification, liquefaction, and landslide and rock fall hazard mapping. Such microzonation maps help make informed decisions for urban planning, and mitigation and adaption for an urban centre or a region.

1.5. Earthquake Site Classification

Earthquake site classification involves categorizing a site into a classification scheme based on site amplification parameters found by site characterization. The principal site amplification parameter is V_S, due to its importance in site amplification estimation and the small variation in material densities. When available, a site is primarily classified according to the time-averaged V_S to a depth of 30 meters (V_{S30}), including in the seismic design provisions of the National Building Code of Canada (NBCC). First introduced by Borcherdt (1994), V_{S30} is widely used as a simple, unambiguous, and easily obtained parameter for site classification (Boore et al., 2011), where the 30 m threshold simply arises from the typical site investigation borehole depth (Anbazhagan, 2011). V_{S30} is

calculated as 30 m divided by the sum of shear wave travel times inside each layer (Borcherdt, 1994):

$$V_{S30} = \frac{30}{\sum(h/V_S)}.$$ (1.3)

V_{S30} is a simplified predictor of earthquake site amplification, where amplification increases as the V_{S30} decreases. It's use is ubiquitous in seismic hazard analysis including ground-motion prediction equations (GMPEs) and building codes worldwide. In Canada, seismic design provisions of the National Building Code of Canada (NBCC) and Canadian Highway and Bridge Design Code (CHBDC) adopted the use of V_{S30} for earthquake site classification in 2000 and 2015, respectively. The site classifications based on V_{S30} used in the NBCC 2010 model are summarised in Table 1.1. To date, amplification hazard mapping is the mapping of V_{S30} measurements or estimates.

Table 1.1. A summary of the seismic site categories in the 2010 NBCC (NRC, 2010)

Site Class	Profile Name	V_{S30} (m/s)
A	Hard rock	$V_{S30} > 1500$
B	Rock	$760 < V_{S30} \leq 1500$
C	Very dense soil and soft rock	$360 < V_{S30} \leq 760$
D	Stiff soil	$180 < V_{S30} \leq 360$
E	Soft soil	$V_{S30} < 180$
F	Other soils	Site-specific evaluation required

Note: A class F is designated for very soft (e.g., peat) conditions where site-specific measurements are required.

1.5.1. Proxy methods for V_{S30}

For regional microzonation studies, site specific V_S profiling can be logistically difficult on a large scale, and so alternative methods have been developed to rapidly approximate V_{S30} on a large scale using a well-known property of the region as a proxy. Mapping using surficial geology as a V_{S30} proxy has been carried out for decades (e.g. Tinsley and Fumal, 1985; Park and Elrick, 1998), in which younger (e.g., Quaternary) geologic units are considered softer and more prone to amplification than older geologic units.

Topographic slope from high resolution Digital Elevation Models (DEM) was proposed as a V_{S30} proxy by Wald and Allen (2007); the steeper the topographic gradient, the stiffer the ground conditions. This methodology was used by the U.S. Geological Survey (USGS) in their generation of a global V_{S30} model (Allen & Wald, 2009). These topographic-slope V_{S30} proxy estimates have been used for seismic hazard and/or risk analyses (e.g., Chaulagain et al. 2015; Sitharam et al. 2015) in lieu of site-specific measurements.

In general, V_{S30}-proxy methods are subject to significant uncertainties regarding local site conditions, namely subsurface impedance contrasts and basin effects (Gallipoli & Mucciarelli, 2009). Allen and Wald (2009) note that the topographic slope proxy method is best used for sites with simple geology and/or significant contrasts in topographic gradient. Thompson et al. (2014) were successful in the integration of topographic data with geology and site-specific measurements for California, but found the map uncertainty to be significantly reduced in areas of denser site-specific measurements. Therefore site-specific measurement is an important part of V_{S30} mapping, even if used in combination with lower-resolution proxy methods.

1.5.2. Alternatives to V_{S30}

In theory, V_{S30} is a simple, easily obtained parameter for site classification (Boore et al., 2011) that describes the average dynamic behaviour of the near surface because of the relationship with the material shear modulus. Because V_{S30} is based on V_S, it is a function of various geological factors (e.g. density, void ratio, effective stress etc.). However there is a lot of discussion as to whether V_{S30} is actually an appropriate parameter for site classification, mostly due to its lack of frequency information and velocity gradient consideration. Boore et al. (1997) noted that V_{S30} is used mainly due to the lack of V_S measurements at greater depths, and suggested the use of average V_S to the depth of one-quarter wavelength instead (Joyner et al. 1981; Boore and Brown 2003). Gallipoli and Mucciarelli (2009) found that V_{S30} failed to predict observed site response for complex geology sites, whereas at simple geology sites, V_{S10} was just as effective as V_{S30}.

An alternative simple measure of site amplification is the Horizontal to Vertical Spectral Ratio (HVSR) peak frequency (f_{peak}) that matches the quarter-wavelength fundamental peak frequency (f_0) of a site (Zhao & Xu, 2013), obtained from either earthquake or microtremor recordings. Zhao and Xu (2003) found f_{peak} to be a more appropriate site response estimator than V_{S30} for deep soil sites. Zhao (2006) proposed a new earthquake site classification based on site period ($1/f_{peak}$) from observed earthquake response spectra at Japanese stations, and Di Alessandro et al., (2012) extended Zhao's site period classification to define site classes for sites with flat HVSRs. Good agreement between earthquake and microtremor HVSRs has been demonstrated at seismic stations in BC (Molnar & Cassidy, 2006; Molnar et al., 2017). Regnier et al. (2014) found that V_{S30} does not account for the complexity of the V_S profile, and suggested the combination of V_S gradient and f_{peak}. Recently, Hassani and Atkinson (2016) demonstrated that V_{S30} can be effectively proxied by f_{peak} from earthquake HVSR and reduce GMPE variability. Braganza et al. (2016) uses only measurements of f_{peak} and mapped surficial geology to produce a regional amplification map of Ontario.

1.6. Organization of work

This thesis consists of two main chapters, which address two important aspects of incorporating site effects and improving seismic hazard assessment in Greater Vancouver.

1.6.1. Chapter 2

The **M** 4.7 Vancouver Island earthquake reoccurred in December 2015 and is the largest recorded inslab earthquake beneath Georgia Strait. Earthquake recordings obtained at strong-motion stations located on varying site conditions offer a significant opportunity to reassess seismic amplification in southwest BC. Additionally this event generated the first earthquake recordings at depth in BC. We examine local variations in the observed spatial variation of ground motion within ~100 km of the epicentre, and investigate how this relates to site effects. High amplification at 4-6 Hz is observed on both thick sediment sites and on the northern edge of the Fraser delta, as observed in previous earthquakes. We conclude that there is a discrepancy between observed ground motions

and current microzonation maps based on surficial geology, suggesting a need for more accurate site classification mapping. This chapter also includes analysis of the first borehole earthquake recordings in British Colombia, obtained in three instrumented boreholes (at surface to 41 m depth) located at the approaches of the Port Mann bridge (~25 km SE of Vancouver). We investigate amplification with depth in the boreholes and estimate shear wave velocity between receivers, obtaining 1D V_S profiles for each borehole.

1.6.2. Chapter 3

To improve earthquake site classification in the region, a greater quantity of site characterizations are required that are based on actual site-specific V_S measurements (high accuracy). Chapter 3 describes the use of passive seismic methods to obtain V_S profiles and important site response parameters (V_{S30}, peak frequency, depths of significant impedance contrasts) at 13 sites in southwest BC, primarily in Greater Vancouver. We also discuss the merits of the passive seismic methodology for site characterization, which offers an attractive alternative to traditional methods due to the speed of acquisition and processing and applicability to urban environments. The success of the passive seismic V_S profiling accomplished at 13 sites of varying geological complexity provides confidence for future earthquake site assessments and serves as the basis for an initiated 5-year seismic microzonation effort in the region.

1.6.3. Chapter 4

Chapter 4 presents a summary of the findings in Chapters 2 and 3. Overall findings of this thesis research are discussed as well as recommendations for future work.

1.7. References

AIR Worldwide. (2013). *Study of Impact and the Insurance and Economic Cost of a Major Earthquake in British Columbia and Ontario/Quebec. Boston, MA.*

Allen, T. I., & Wald, D. J. (2009). On the Use of High-Resolution Topographic Data as a Proxy for Seismic Site Conditions (VS30). *Bulletin of the Seismological Society of*

America, *99*(2A), 935–943. http://doi.org/10.1785/0120080255

Anbazhagan, P. (2011). *Introduction to Engineering Seismology. National Programme on Technology Enhanced Learning (NPTEL)*. National Programme on Technology Enhanced Learning (NPTEL).

Balfour, N. J. (2011). *Sources of Seismic Hazard in British Columbia: What Controls Earthquakes in the Crust?* University of Victoria.

Bent, A. L., & Greene, H. (2012). *Recurrence Rates and b Values for Global In-slab Earthquakes. Open file (Geological Survey of Canada)*.

Boore, D. M., Joyner, W. B., & Fumal, T. E. (1997). Equations for estimating horizontal response spectra and peak acceleration from western North American earthquakes: a summary of recent work. *Seismological Research Letters*, *81*(1), 128–153.

Boore, D. M., Thompson, E. M., & Cadet, H. (2011). Regional correlations of V s30 and velocities averaged over depths less than and greater than 30 meters. *Bulletin of the Seismological Society of America*, *101*(6), 3046–3059. http://doi.org/10.1785/0120110071

Borcherdt, R. D. (1994). Estimates of Site- Dependent Response Spectra for Design (Methodology and Justification). *Earthquake Spectra*. http://doi.org/10.1193/1.1585791

Chaulagain, H., Rodrigues, H., Silva, V., Spacone, E., & Varum, H. (2015). Seismic risk assessment and hazard mapping in Nepal. *Natural Hazards*, *78*(1), 583–602. http://doi.org/10.1007/s11069-015-1734-6

Clague, J. J. (1997). Earthquake hazard in the Greater Vancouver area. *Environmental Geology of Urban Areas, Geological Society of Canada*, 285–296.

CREW. (2011). History Of Earthquakes In Cascadia. Retrieved August 11, 2017, from http://www.crew.org/earthquake-information/history-of-earthquakes-in-cascadia

Di Alessandro, C., Bonilla, L. F., Boore, D. M., Rovelli, A., & Scotti, O. (2012). Predominant-Period Site Classification for Response Spectra Prediction Equations in Italy. *Bulletin of the Seismological Society of America*, *102*(2), 680–695. http://doi.org/10.1785/0120110084

Gallipoli, M. R., & Mucciarelli, M. (2009). Comparison of Site Classification from VS30, VS10, and HVSR in Italy. *Bulletin of the Seismological Society of America*, *99*(1), 340–351. http://doi.org/10.1785/0120080083

Hassani, B., & Atkinson, G. M. (2016). Applicability of the NGA- West2 Site- Effects Model for Central and Eastern North America. *Bulletin of the Seismological Society of America*, *106*(3), 1331–1341. http://doi.org/10.1785/0120150321

Jackson, F., Molnar, S., Ghofrani, H., Atkinson, G. M., Cassidy, J. F., & Assatourians., K. (2017). Ground Motions of the December 2015 M 4.7 Vancouver Island Earthquake: Attenuation and Site Response. *Bulletin of the Seismological Society of America, Accepted.*

Molnar, S., Braganza, S., Farrugia, J., Atkinson, G., Boroschek, R., & Ventura, C. (2017). Earthquake site class characterization of seismograph and strong-motion stations in Canada and Chile, (January).

Molnar, S., & Cassidy, J. F. (2006). A Comparison of Site Response Techniques Using Weak-Motion Earthquakes and Microtremors. *Earthquake Spectra*, *Vol. 22*(1), 169–188.

Molnar, S., Crow, H., Ventura, C., Finn, W., & Stokes, T. (2014). Regional seismic hazard assessment for small urban centers in Western Canada. *In Proceedings of the 10th National Conference in Earthquake Engineering*.

Molnar, S., Dosso, S. E., & Cassidy, J. F. (2010). Bayesian inversion of microtremor array dispersion data in southwestern British Columbia. *Geophysical Journal International*, *183*(2), 923–940. http://doi.org/10.1111/j.1365-246X.2010.04761.x

Molnar, S., Dosso, S. E., & Cassidy, J. F. (2013). Uncertainty of linear earthquake site amplification via Bayesian inversion of surface seismic data. *Geophysics*, *78*(3), WB37-WB48.

National Research Council (NRC). (2010). National Building Code of Canada. Associate Committee on the National Building Code, National Research Council of Canada, Ottawa, Ontario.

Natural Resources Canada. (2016). Earthquake Hazards and Risks. Retrieved August 7, 2017, from http://www.earthquakescanada.ca/hazard-alea/earthquake_hazards_risks.pdf

Panza, G., Pakaleva, I., & Nunziata, C. (Eds.). (2004). Seismic ground motion in large urban areas. *Springer Science & Business Media. Chicago.*

Park, S., & Elrick, S. (1998). Predictions of shear-wave velocities in southern California using surface geology. *Bulletin of the Seismological Society of America*, *88*(3), 677–685.

Regnier, J., Bonilla, L. F., Bertrand, E., & Semblat, J.-F. (2014). Influence of the VS Profiles beyond 30 m Depth on Linear Site Effects: Assessment from the KiK-net Data. *Bulletin of the Seismological Society of America*, *104*(5), 2337–2348. http://doi.org/10.1785/0120140018

Sánchez-Sesma, F. J. (1987). Site effects on strong ground motion. *Soil Dynam. Earthquake Eng.*, *6*(2), 124–132. http://doi.org/10.1016/0267-7261(87)90022-4

Satake, K., Wang, K., & Atwater, B. F. (2003). Fault slip and seismic moment of the 1700 Cascadia earthquake inferred from Japanese tsunami descriptions. *Journal of Geophysical Research*, *108*(B11), 2535. http://doi.org/10.1029/2003JB002521

Seed, H. B., & Idriss, I. M. (1970). Soil moduli and damping factors for dynamic response analysis. *Journal of Terramechanics*. http://doi.org/10.1016/0022-

4898(72)90110-3

Seed, H. B., Romo, M. P., Sun, J. I., Jaime, A., & Lysmer, J. (1988). The Mexico Earthquake of September 19, 1985—Relationships Between Soil Conditions and Earthquake Ground Motions. *Earthquake Spectra*, *4*(4), 687–729. http://doi.org/10.1193/1.1585498

Sitharam, T. G., Kolathayar, S., & James, N. (2015). Probabilistic assessment of surface level seismic hazard in India using topographic gradient as a proxy for site condition. *Geoscience Frontiers*, *6*(6), 847–859. http://doi.org/10.1016/j.gsf.2014.06.002

Steven Earle. (2016). *Physical Geology*. CreateSpace Independent Publishing Platform .

Thompson, E. M., Wald, D. J., & Worden, C. B. (2014). A VS30 Map for California with geologic and topographic constraints. *Bulletin of the Seismological Society of America*, *104*(5), 2313–2321. http://doi.org/10.1785/0120130312

Tinsley, J., & Fumal, T. (1985). Mapping Quaternary sedimentary deposits for areal variations in shaking response. *Valuating Earthquake Hazards in the Los Angeles Region—An Earth Science Perspective, 1360, 101-126.*

Wald, D. J., & Allen, T. I. (2007). Topographic slope as a proxy for seismic site conditions and amplification. *Bulletin of the Seismological Society of America*. http://doi.org/10.1785/0120060267

Worden, C. B., & Wald, D. J. (2016). ShakeMap manual online: technical manual, user's guide, and software guide. *US Geol. Surv. Chicago.*

Zhao, J. X., & Xu, H. (2013). A Comparison of V_{S30} and Site Period as Site-Effect Parameters in Response Spectral Ground-Motion Prediction Equations. *Bulletin of the Seismological Society of America*, *103*(1), 1–18. http://doi.org/10.1785/0120110251

Chapter 2

2.   Observed site response of the 30 December 2015 M 4.7 Vancouver Island earthquake

2.1.   Introduction

The 29 December 2015 (11:39pm Pacific Time) moment magnitude (**M**) 4.7 Vancouver Island earthquake was a normal-faulting event at 60 km depth within the subducting Juan de Fuca oceanic plate (i.e. an inslab event), whose epicentre (48.62°N, 123.30°W) is located approximately 21 km NNE of Victoria and 71 km SSW of Vancouver, BC. Despite its small magnitude, the earthquake was felt to a distance of about 150 km in all directions across much of BC's South Coast and parts of Washington State; ~7000 online felt responses were submitted on the Earthquakes Canada website, and ~14,000 online felt responses were submitted to the U.S. Geological Survey's 'Did You Feel It' website. This event is noteworthy to the region due to its magnitude and location, as the fourth recorded inslab earthquake greater than magnitude 4 to have occurred in the Georgia Strait (epicentre within 50 km of Victoria). Inslab earthquakes exhibit the greatest frequency of occurrence in Cascadia, being more frequent than crustal or interface events. Thus they are a significant contributor to short-period ground shaking hazard in the region due to their frequency of occurrence.

The west coast of BC is well instrumented due to the high seismic hazard from the Cascadia subduction zone, and there has been significant expansion in strong-motion monitoring over the last 15 years (Cassidy et al. 2007; Cassidy et al. 2015). Following the 2001 Nisqually earthquake, the Geological Survey of Canada (GSC) – a division of Natural Resources Canada (NRC) - designed low-cost near-real-time internet accelerometers (IAs) that revolutionized strong-motion monitoring in BC (Rosenberger et al. 2007). As of 2017, NRC together with the BC Ministry of Transportation and Infrastructure (BC MoTI) and the Miller Capilano Highway Maintenance Corporation operate a total of 105 strong motion instruments in southwest BC as part of the national strong motion network (http://www.earthquakescanada.nrcan.gc.ca/stndon/CNSN-

RNSC/sm/sm_west_maplist-en.php/). In addition to this network, BC Hydro currently operates ~80 instruments strong-motion instruments at dams and substations across BC. All near-real-time IA strong-motion monitoring in BC is available via the BC Smart Infrastructure Monitoring (BCSIMS; www.bcsims.ca) project (Kaya et al. 2014). Most recently, ~30 schools in the Lower Mainland region have had strong-motion instrumentation installed as part of an earthquake early warning system (Ventura et al., 2016). Because of this recently increased density of strong-motion instrumentation in southwest BC, the 2015 **M** 4.7 inslab earthquake is a notably recorded event. Additionally, as part of the construction of the Port Mann Bridge in 2012, BC MoTI deployed downhole arrays at terminus ends of the bridge featuring three strong motion instruments within each instrumented borehole. This means the 2015 event is the first to be recorded in boreholes at depth in BC.

2.1.1. Aims and Objectives

The goal of this chapter is to examine local variations in the 2015 **M** 4.7 earthquake shaking related to mapped geology and current seismic microzonation mapping (site effects) from strong-motion recordings within ~100 km of the epicentre. This chapter also includes site amplification and cross-correlation analysis for 1D V_S profiling from the first earthquake recordings obtained in three instrumented boreholes (at surface to 41 m depth) located along the Trans-Canada Highway 1 at the approaches of the Port Mann bridge spanning Coquitlam and Surrey, BC (~25 km SE of Vancouver).

2.2. Local geology and site amplification

2.2.1. Greater Vancouver

The Greater Vancouver area consists mostly of Pleistocene glacial and interglacial sediments overlying Tertiary bedrock of the Georgia Basin. Bedrock consists of Miocene sandstones and shales, with a shear wave velocity (V_S) of 2-3.5 km/s (Monahan & Levson, 2000b). The bedrock depth varies from ~200 m north of the Fraser River to ~800 m southward below Ladner (Britton et al., 1995).

Overlying this, Pleistocene sediments cover much of the Greater Vancouver area and consist of mostly fine sands and interbedded silts of glacial and interglacial origin, with a thickness of up to 500 m in the centre of the delta (Britton et al., 1995). The average V_S of the Pleistocene sediments varies from 0.4-1.1 km/s with no known relationship between velocity and depth (Hunter & Christian, 2001). Molnar et al. (2014a,b) demonstrated that the ~5-km deep Late-Cretaceous Georgia basin, infilled with sedimentary rock and these Pleistocene glacial deposits, increases long-period ground motions by an average factor of 3-4 in Greater Vancouver.

In addition to the Pleistocene sediments, are the thick unconsolidated Holocene sediments comprising the Fraser delta, south of Vancouver. The loose Holocene silts, sands and clays, exhibit an average V_S between 200-300 m/s, which increases with depth due to sedimentary loading (Hunter et al., 1998). The Holocene-Pleistocene boundary is thus marked by a significant contrast in V_S. Holocene age Fraser delta sediments reach thicknesses of 300 m (Hunter et al., 1997) in the centre of the delta. These deltaic sediments were deposited over the last 11,000 years since the last glaciation (Clague, 1998) and are generally fine grained and unconsolidated.

These delta sediments are well recognized as subject to high amplification and liquefaction due to their significant thickness, relatively low seismic velocity and presence of saturated channel sands (Monahan et al., 1993; Hunter et al., 1998). Cassidy and Rogers (2004) observed frequency dependent spectral amplification from three moderate-to-large earthquakes at 1.5-4 Hz with a factor of up to 12 times that of competent bedrock near the Holocene delta edge. Near the delta centre, peak amplification is a factor of 4-10. At deep delta sites, amplification up to factor of 3 (relative to vertical motions) is consistently observed at low ~0.3 Hz frequency from weak-motion earthquake and ambient vibration (microtremor) recordings due to the presence of the thick Holocene sediments (Molnar et al., 2013).

2.2.2. Greater Victoria

The geology of Greater Victoria consists of glaciomarine clays and Holocene organic soils overlying Pleistocene tills and Lower Paleozoic to Eocene bedrock (Monahan & Levson, 2000b). Glacial scouring has produced an irregular topography and a variable depth to bedrock between 0 and 30 m. The igneous and metamorphic bedrock ranges in age from Lower Paleozoic to Lower Cenozoic, and has an average V_S of 2-3.5 km/s (Monahan & Levson, 1997). Overlying this are over consolidated Pleistocene tills with an average V_S of 500 m/s (Monahan & Levson, 1997). In some areas, glacial meltwater has deposited soft marine clay known as the 'Gray Victoria clay'. In some places this has been further weathered into 'Brown Victoria clay', which is hardened from oxidation and desiccation. The gray and brown clays have average V_S of 132 m/s and 213 m/s respectively (Monahan & Levson, 1997).

Site amplification in Victoria is mostly due to these glaciomarine clays: the brown clay at depths of less than 15 m and the gray clay have been assigned National Building Code of Canada (NBCC) site classes of D and E respectively, or stiff soil and soft soil (Monahan et al. 2000). Ground motions from the 2001 Nisqually earthquake exhibit a relatively flat response at frequencies < 10 Hz in thin soil sites (< 3 m), whereas peak amplitudes occur at 2-5 Hz in thicker soil sites (5-11 m) (Molnar et al., 2004). The site amplification observed in Victoria from the 2001 Nisqually earthquake is consistent with other earthquakes at various azimuths and depths (Molnar et al., 2007) as well as with microtremor recordings (Molnar & Cassidy, 2006).

2.3. Strong Motion Analysis

2.3.1. Dataset

Strong-motion recordings of the 2015 **M** 4.7 Vancouver Island earthquake were obtained from the BCSIMS strong-motion IA network (see Data and Resources section). Time-series are available from 56 strong-motion stations operating within 100 km of the earthquake epicentre. Ground motions at further distances are unlikely to exceed the site

background and instrument's noise (e.g., Figure 2.3); waveforms available at further distance stations are not considered further here. Basic waveform processing is performed using the ObsPy toolbox for Python (Beyreuther et al., 2010). We remove the mean and trend from the time series, apply a 10% cosine taper and perform instrument correction. A bandpass Butterworth filter is applied between 0.1 and 20 Hz, and the horizontal components are rotated into radial and transverse components. PGA at each of these stations is shown in Figure 2.1. The 2015 **M** 4.7 earthquake was also recorded by the three downhole arrays at both terminus ends of the Port Mann bridge (labelled B1 to B3 in Figure 2.1). These strong-motion borehole recordings provide the first opportunity to examine the variation of earthquake shaking amplitude with depth in the Lower Mainland.

2.3.2. Spatial variation of ground motions

Peak ground acceleration reached a maximum of 4.45% g in Greater Vancouver (Figure 2.1) and 4.65% g in Greater Victoria (Figure 2.2). To investigate the effects of local geology in Vancouver, we overlay pre-existing amplification hazard estimates of Victoria (Monahan et al. 2000) and Greater Vancouver (Monahan, 2005), derived from geological mapping with assigned National Building Code of Canada (NBCC; 2005). To examine the spatial variation of the observed ground motions, we examine approximately north-south trending transects of acceleration down the spine of Greater Victoria (Transect 1 in Figure 2.3) and across the Fraser delta (Transects 2 and 3 in Figure 2.3). The transverse-component recordings, zoomed to display the shear wave arrivals, are shown in Figure 2.4, with background shading corresponding to amplification hazard class. For transect stations near Victoria (Figure 2.4a), amplification hazard rating is assigned here by S. Molnar from knowledge of geologic conditions and/or previous ambient site amplification measurements.
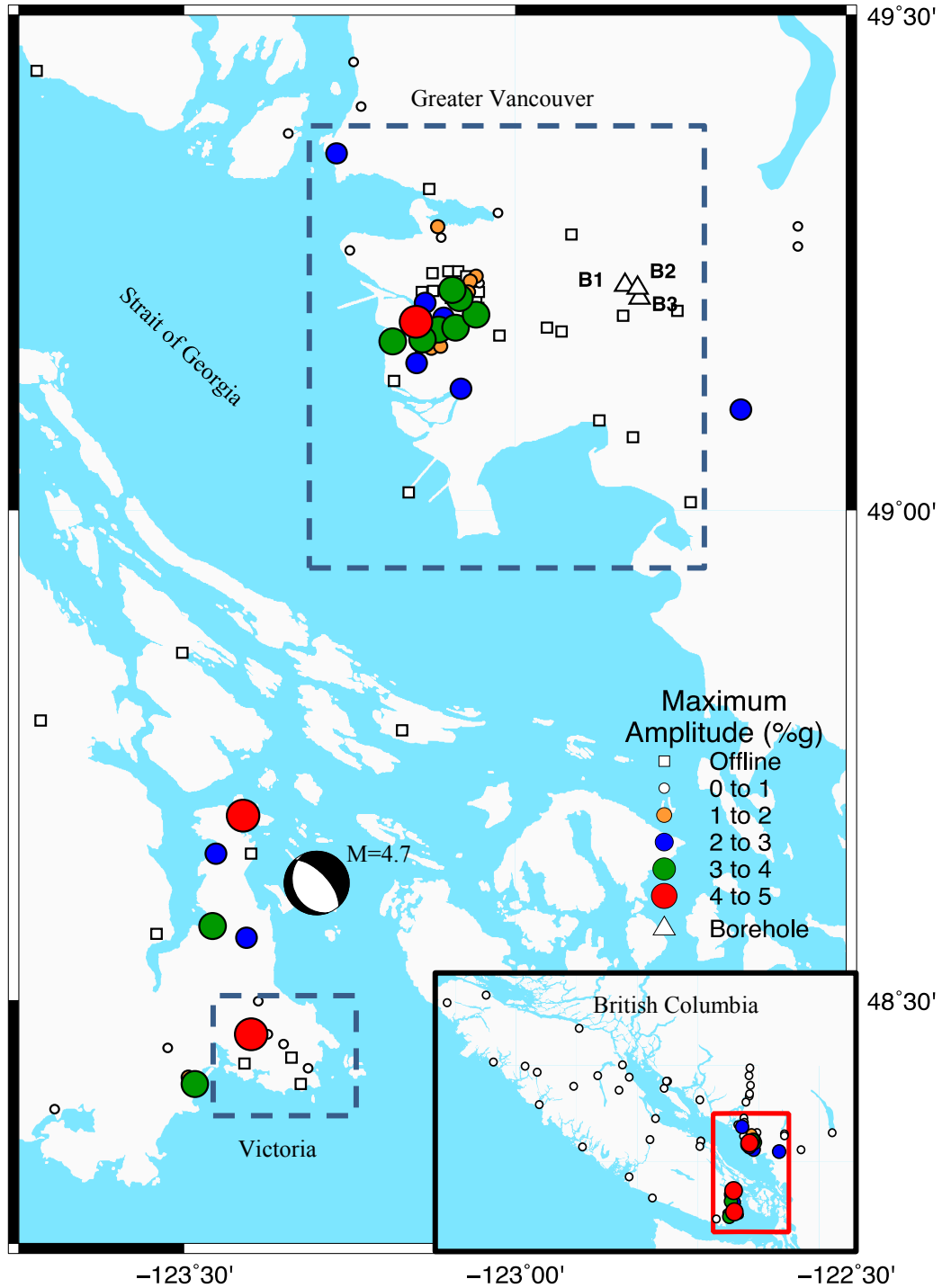
Figure 2.1. Variation in peak ground acceleration at strong motion stations across southwest BC are shown by filled circles. The M 4.7 earthquake focal mechanism (beach ball) denotes the earthquake epicentre and locations of three borehole arrays (B1-B3) are shown by triangles.
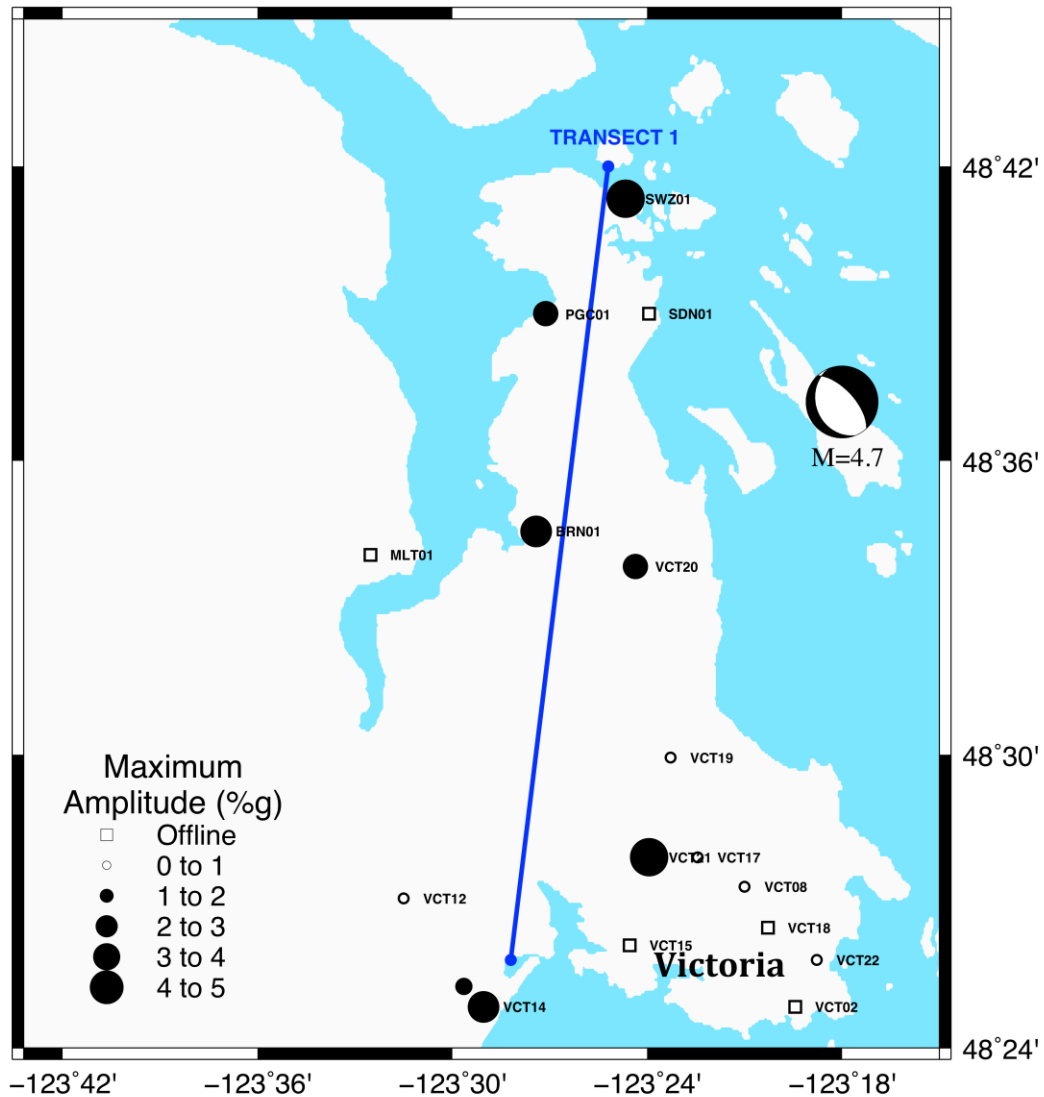
Figure 2.2. Variation in peak ground acceleration at strong motion stations in southern Vancouver Island. Seismic waveforms shown in Figure 2.4 are selected along N-S transect shown by the solid line.
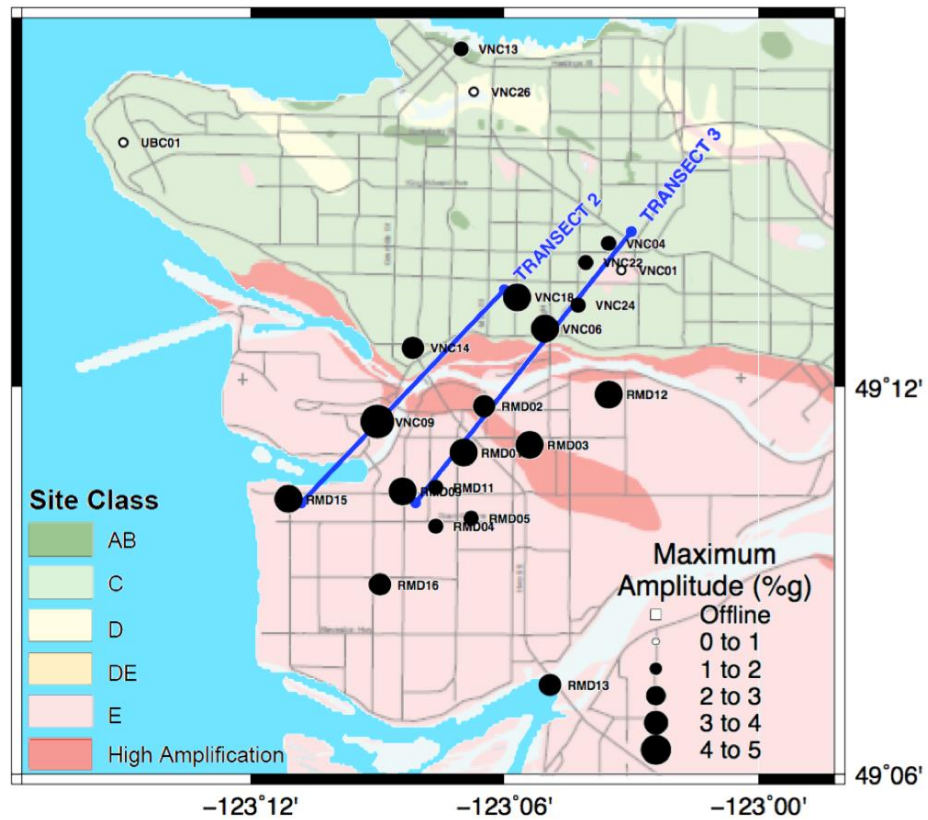
Figure 2.3. Variation in peak ground acceleration at strong motion stations in southwest Greater Vancouver. Seismic waveforms shown in Figure 2.4 are selected along two NE-SW transects shown by the solid lines. Background shading corresponds to amplification hazard rating, modified from Monahan (2005).
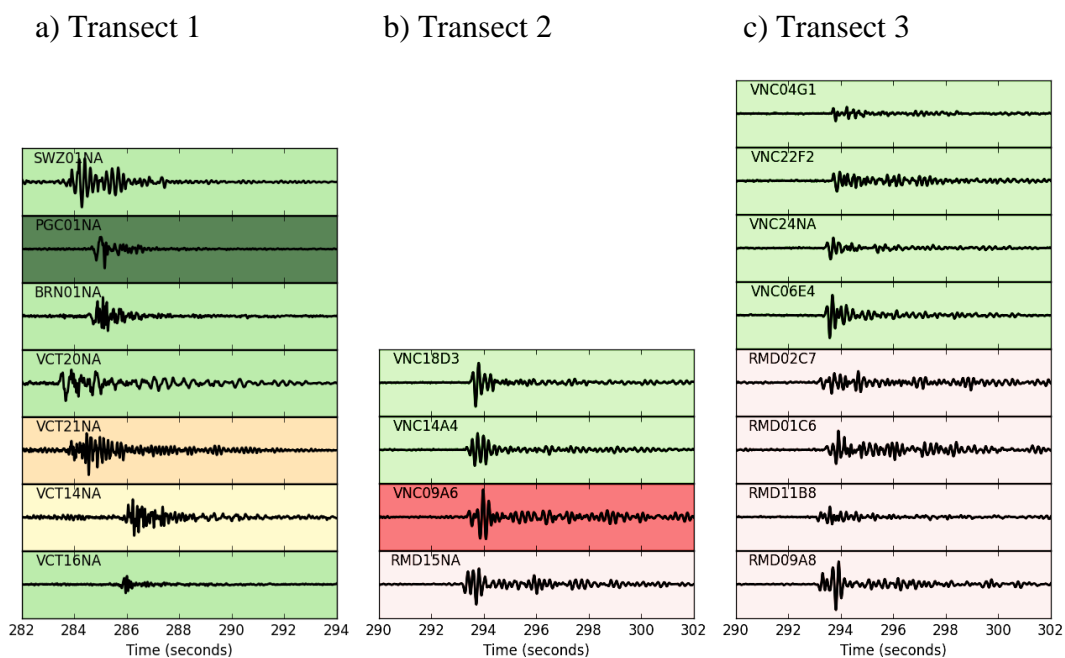
Figure 2.4. Transverse component seismic waveforms along transects labelled in Figure 2.2 and Figure 2.3. Y-axis is acceleration in units of g, plotted to ± 0.05 g. Background shading corresponds to amplification hazard site class assigned by S. Molnar for Victoria stations and Monahan (2005) for Vancouver stations as in Figure 2.2.

Figure 2.4 demonstrates variability in the recorded ground motions: amplitudes, predominant frequencies, and durations of body shear wave and surface wave content. For example Stations at the northern end of Saanich Peninsula (SWZ, PGC, BRN; Figure 2.2) are closest (10 km) to the epicentre. Of these, PGC is located on quartz diorite bedrock, whereas SWZ and BRN are located on unknown site conditions at the BC Ferries Swartz Bay terminal and a private residence in Brentwood Bay, respectively. The larger amplitudes observed at the ferry terminal are not observed at the PGC rock and Brentwood Bay stations (Figure 2.4a). The central Saanich (VCT20) station is located within 500 m of BC Hydro's Keating electrical substation. The known geological conditions at Keating substation is ~10 m clay over glacial till with hard crystalline bedrock at ~30 m depth (Molnar et al., 2004). Site amplification at 2-4 Hz was observed

at Keating during the Nisqually earthquake (Molnar et al., 2004) and is consistent with the waveform at VCT20 in Figure 2.4a. The waveform at VCT21 shows high-frequency (~5 Hz) ringing. This station is located on an unknown thickness of Victoria clay along a two-lane road near Colquitz creek (topographic low) below a four-lane overpass. In Colwood, VCT14 and VCT16 are located on the Colwood sand and gravel delta outwash plain and a small rock outcrop, respectively. This is consistent with the observed waveforms in Figure 2.4a.

In Vancouver (VNC stations), over 50 km distance from the epicentre, ground motion amplitudes (e.g., Transect 2 in Figure 2.4b) are similar to those closer to the epicentre. We expect reduced amplitudes in Vancouver, due to the increased distance and presence of relatively stiff Pleistocene post-glacial sediments (e.g. VNC04, 22, 24). As we examine the waveforms at stations further south along Transects 1 and 2, we observe increasing PGA on the Holocene Fraser River delta sediments, with observed maximum amplitudes along Transect 1 at VNC09 (4.45% g) and Transect 2 at RMD09 (3.77% g), which is consistent with observations from previous earthquakes (Cassidy & Rogers, 1999) and microtremor (Onur et al., 2004) studies. It is noteworthy to mention however that the strongest amplification occurs at the sites on the northern edge of the delta, where the Holocene sediment is not at its thickest. Cassidy and Rogers (2004) also noted high amplitudes here, and attributed this to the thickness of the Holocene and Pleistocene sediments being favorable to amplify the dominant frequency of the source spectra. Other deviations from the general trend (e.g., VNC14 or RMD02 and cluster of RMD04, 5, 11 respectively) are also worth noting. These nonconformities demonstrate that the bi-modal "stiff Vancouver" and "soft Fraser River delta site amplification mapping is a gross generalization compared to site-specific recordings of earthquake shaking.

We calculate the Fourier amplitude spectra of the **M** 4.7 earthquake recordings at five select locations (Figure 2.5). Spectra are computed for tapered 40 s time windows of the accelerograms, beginning 2 s before the S-wave arrival. Each spectrum is smoothed using a Konno and Ohmachi (1998) smoothing function with a frequency bandwidth coefficient of 40. This creates an approximating function that ignores unwanted noise using a moving average. The Konno and Ohmachi function is often recommended for frequency

analysis as it acts on a constant width in either logarithmic or linear frequency scales, and ensures a constant number of points at all frequencies (Konno and Ohmachi, 1998). The decay of amplitude due to geometric spreading is corrected for hypocentral distance (R_{hypo}) based on body-wave attenuation (i.e., $1/ R_{hypo}$). Fourier spectra at these locations have been examined from previous earthquake recordings (Cassidy & Rogers, 2004) and demonstrated amplification at both thick and delta-edge Fraser River delta sites; the frequency band of the amplified motions varies among earthquakes. The acceleration spectra of sites in the Fraser delta from the **M** 4.7 event is consistent with previous earthquakes, demonstrating the strongest amplification at both thick-delta (RMD13) and delta-edge (RMD02, RMD09, VNC14) sites in the 4-6 Hz frequency band.
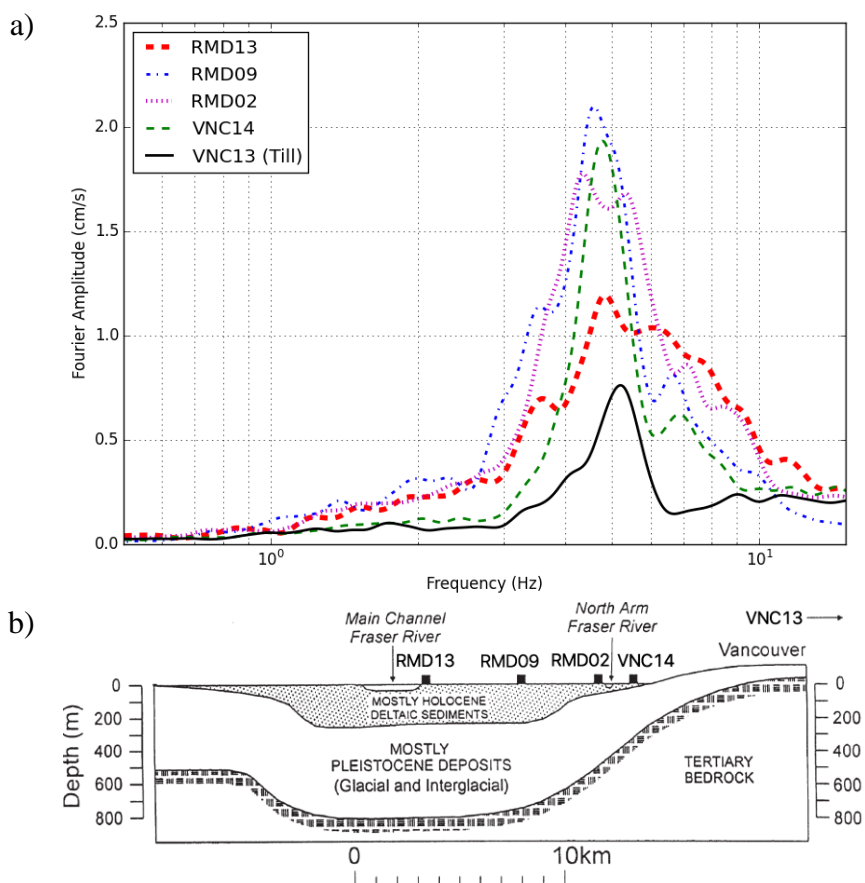
Figure 2.5. (a) Transverse-component Fourier acceleration spectra at select IA stations across the Fraser delta, compared to a station on Pleistocene till in downtown Vancouver (VNC13). (b) Cross-section of the Fraser River delta with select strong-motion stations labelled and shown by black squares (modified from Cassidy and Rogers, 1999).

2.3.3. Borehole array recordings

Three borehole arrays exist at terminus ends of the Port Mann bridge; boreholes 2 and 3 beneath the north and south bridge approaches, respectively, and borehole 1 is 900 m west of borehole 2. Each borehole array is comprised of three tri-axial accelerometers, installed between the surface and 57 m maximum depth. Table 2.1 reports depth of each installed sensor and summarizes stratigraphic information between installation depths of the three borehole arrays.

Table 2.1. Stratigraphic summary of the borehole arrays.

Borehole	Sensor Name	Depth	PGA[+] (% g)	Approx. thickness and soil type
1	PMB10	-4 m	16.30	3 m landfill/peat
				5.5 m dense sand
				5 m firm clayey-sandy silt
	PMB11	9 m	7.69	25 m dense sand
				2 m v. dense sandy gravel
				3 m till
	PMB12	41 m	5.01	Till
2	PMB02	2 m	4.57	2 m brown sand
				2 m grey silt/peat
				23 m grey sand
				1 m gravel & cobbles
				5 m grey clay
	PMB01	36 m	3.10	5 m grey clay with gravel
				5 m grey silt & sand
	PMB03	46 m	3.51	(Till)
3	PMB04	16 m	5.47	13.5 m grey sand
				3.5 m grey clayey silt
	PMB05	33 m	6.72	2.5 m grey silt
				2.5 m silt, gravel
				1.5 m coarse sand & gravel
				3.5 m grey silt & clay
				11 m grey clay
				3 m sand with gravel
	PMB06	57 m	4.53	(Till)

[+]PGA is the geometric mean of the two horizontal components.

The surface accelerometer at borehole 1 is installed on a concrete pad 4 m higher than boreholes 2 and 3. Borehole 1's installation depths and stratigraphic profile are provided by BCSIMS; sensors are installed at geology contrasts. Stratigraphic information

surrounding boreholes 2 and 3 was obtained from P. Monahan (pers. comm., 2016). The depth of glacial till in these supplemental borehole logs at the north (borehole 2) and south (borehole 3) terminus of the bridge is ~50 m and ~60 m, respectively. Hence, we are reasonably confident that the deepest (third) sensor in all three borehole arrays is located within Pleistocene glacial till (i.e., base of Holocene Fraser delta). In general, the amplitude of recorded motions within the borehole arrays (Table 2.1) is similar or higher than at nearby surface stations (Figure 2.1). An expected increase in amplitude towards surface (amplification) in these deltaic sediment boreholes is generally observed. The largest amplitudes are observed at surface (PMB10).

2.3.4. Site amplification with depth

We examine alterations in the recorded motions and the frequencies (or periods) at which de/amplification of the S-wave arrival occurred using spectral ratio analyses. Two spectral ratio analyses are performed using the borehole array recordings: horizontal-to-vertical, and various reference combinations within the borehole (i.e., lower-to-upper, lower-to-middle, middle-to-upper sensor). The three arrays are relatively close with similar geology (Table 2.1), although borehole 3 is located on the opposite (south) side of the Fraser River. The depth to stiff glacial till increases southward from borehole 1 (~38 m) to borehole 3 (~55-60 m).

Figure 2.6 displays the HVSR of the S-wave arrival obtained at each instrumented depth of the three borehole arrays. First a 40 second time window beginning 2 seconds before the S-wave arrival is extracted from each time series, and the quadratic mean of the two horizontal spectra at each station is normalized by the vertical spectrum to obtain the HVSR. Peak amplification between the three holes is relatively consistent, occurring between 0.65 - 0.9 Hz. All three cases demonstrate that the fundamental peak frequency is observed with moderate (4-6) amplification at the base of each instrumented borehole (41-57 m depth), which is highly amplified approaching and at surface. The HVSR results of boreholes 1 and 2 are more similar to each other (on the north side of the Fraser River) than to borehole 3 (on the south side). Amplification occurs at higher frequencies

in boreholes 1 and 2 where the depth to glacial till is shallower than borehole 3 on the south side of the Fraser River.
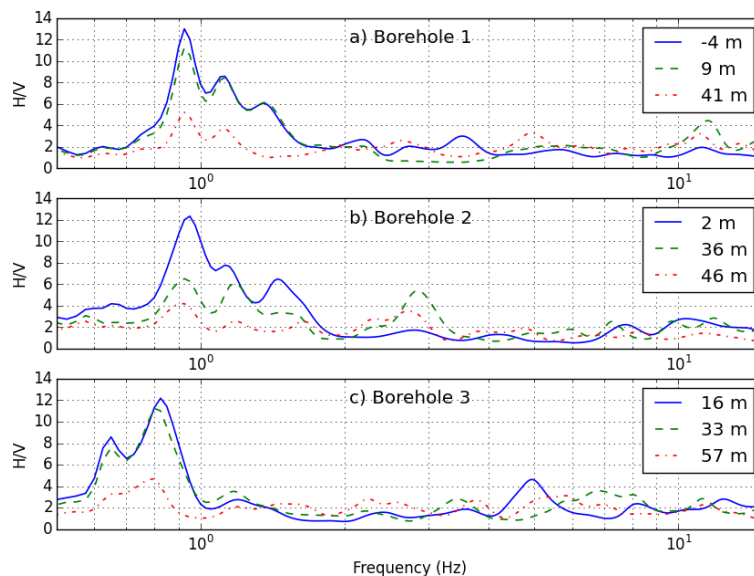
Figure 2.6. Earthquake HVSRs obtained at particular depths within the three borehole arrays.

In general, spectral ratios using borehole records can remove the need for a separate hard rock site that may be far away, and can thus eliminate the disparities between the wavefield at the two sites. If the receiver at the bottom of the borehole is inside a seismically hard layer, and the surface receiver is on soft sediment where we expect amplification, we can take the surface to bottom ratio between the two as a measure of site amplification. Because the hard reference site is at the same location, we can be confident that the wavefield is the same, resulting in accurate spectral ratios. The drawback of this technique is that because of the free surface involved, the surface-to-depth-within-borehole spectral ratios require correction of the destructive interference involved in the down-going wave effect (Bonilla et al., 2002). If uncorrected, the spectral ratios exhibit gaps in the downhole spectra. Despite this drawback, we compute the three possible upper-to-lower spectral ratio combinations using the same processing methodology used for calculating HVSRs. Figure 2.7 shows the combinations of borehole ratios calculated for the eastern component of each borehole (northern component response is similar and not shown here for brevity).

These upper-to-lower spectral ratios clearly demonstrate at which frequencies the seismic waves are amplified towards surface. In borehole 1 (Figure 2.7a), the three largest peaks in the spectral ratio between the top and bottom sensors (solid line) occur at 1.4 Hz, 3.5 Hz and 7.9 Hz. The 1.4 Hz peak is detected between 9 and 41 m, but not between the surface and 9 m, suggesting that this amplification is generated at depth and/or within this lower depth interval and is the lowest observed peak frequency. Conversely, the two higher frequency peaks are generated between surface and 9 m. These higher frequency peaks likely correspond to amplification by the soft landfill/peat, clayey silt and dense sand that comprise the upper 7 m of this borehole.
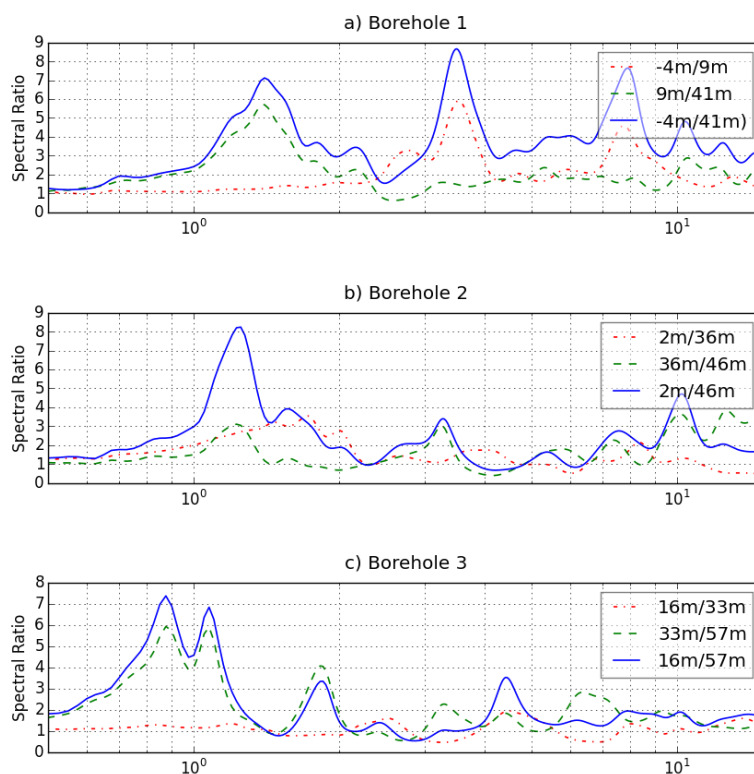
Figure 2.7. Upper-to-lower spectral ratios (depths are reported in each legend) determined within each borehole array.

In borehole 2 (Figure 2.7b), peak amplification occurs at 1.2 Hz, with lower amplification observed at multiple higher frequencies. The lowest frequency peak at 1.2 Hz again appears to be generated at depth (present in the lower portion of the borehole) and is amplified towards surface. It appears that the contribution of the upper 2-36 m depth interval of borehole 2 generates amplification at 1.5-2 Hz, amplifying the 'right shoulder'

of the lower fundamental peak. Lastly, we note that the depth ranges of the upper-to-lower ratios between boreholes 1 and 2 are not directly comparable (i.e. sample different depth ranges).

Borehole 3 features a double peak between 0.9 and 1.1 Hz, and like the other two previous boreholes, this is prominent in the lower portion (33-57 m depth) of the borehole. The ratio in the "upper" 16-33 m depth interval of the borehole is fairly flat through the entire frequency range, which suggests a lack of impedance contrast between these depths. Unlike the other two boreholes there are no significant high frequency peaks (> 6 Hz), likely due to the first sensor located at 16 m depth.

2.3.5. Downhole cross correlation analysis

To obtain 1D V_S profiles of the Port Mann Bridge borehole arrays, we performed cross-correlation analysis between pairs of recordings within each borehole. This technique identifies the quantitative time delay of the correlated (direct S-wave) signal between pairs of recordings. Based on the relatively deep depth of this event, shear waves are assumed to travel vertically and therefore the time delay in shear wave propagation provides an estimation of V_S, assured by the high sampling rate (100 Hz). We calculate the cross correlation between the upper and lower borehole recording pairs of each array using a maximum shift length of 5000 samples (50 s). From the known distance (depth) between recordings, and the obtained cross-correlated time delay, we determine V_S at two depth intervals traversed within the boreholes (Figure 2.8). The cross-correlation analysis allows us to build a useful picture of the interval V_S along the instrumented borehole length. The estimated V_S depth profiles indicate low velocities in all three boreholes, as expected in the Holocene silts sands and clay of the Fraser delta. The lowest measured V_S occurs near surface (upper 13 m of borehole 1). The transition between the upper sands and lower clays in borehole 3 is marked by a reduction in V_S.
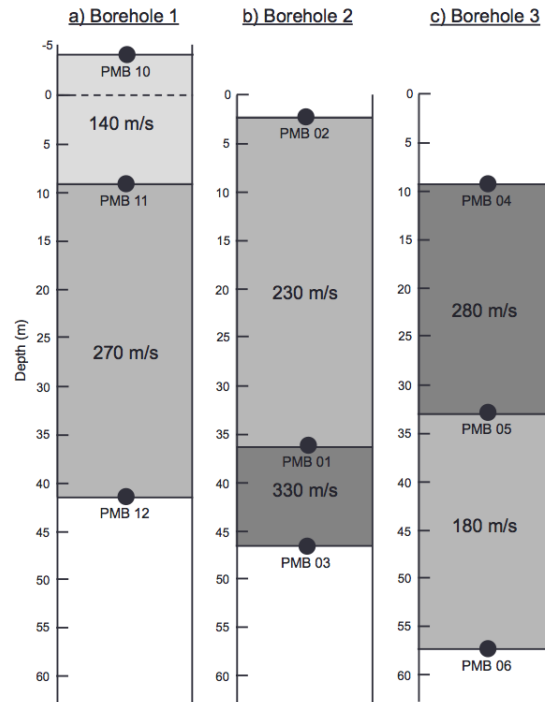
Figure 2.8. Interval V$_S$ determined within each borehole arrays. Black dots correspond to sensor depth.

2.4. Conclusions

The 2015 **M** 4.7 Vancouver Island inslab earthquake was recorded by a relatively dense strong-motion network, and the available recordings of this earthquake provide a significant opportunity to re-evaluate local variations in the shaking related to geology and/or site effects in southwest British Columbia. There is clear variability in the amplitude, dominant frequencies and durations of recorded ground motions. The distribution of observed amplification generally agrees with previous earthquakes, where high amplification is observed at 4-6 Hz on both thick sediment sites and on the northern edge of the Holocene Fraser Delta. Reduced amplitudes are observed in Vancouver, where stations sit on relatively stiff Pleistocene post-glacial sediments. We conclude that site amplification was a major factor that caused this event to be felt strongly. The spatial distribution of observed amplification generally agrees with previous earthquakes, where high amplification is observed on both thick sediment sites and on the northern edge of the Holocene Fraser delta. This study illustrates some local discrepancies at a higher

spatial resolution in comparison to current regional seismic microzonation maps (Monahan, 2005; Monahan et al., 2000), which are based on limited local geological and geotechnical information. Furthermore geological boundaries are mostly defined by the surface distribution, rather than the subsurface. Consequently current microzonation maps capture gross generalizations but do not predict the observed variable earthquake shaking.

Recordings at various depths within three borehole arrays beneath the Port Mann Bridge provide information about amplification and average shear wave velocity with depth. The maximum observed amplification within the three borehole arrays is a consistent factor of 7-8, corresponding to the relatively consistent 40-45 m depth interval of Holocene Fraser delta sediments. Average V_S determined at two depth intervals within each borehole are < 350 m/s, which is expected of Holocene Fraser delta sediments.

2.5. Data and Resources

Reported total number of felt reports on the U.S. Geological Survey and Earthquakes Canada event websites were obtained from http://earthquake.usgs.gov/earthquakes/eventpage/uw61114971#dyfi (last accessed 15 February 2017) and http://www.earthquakescanada.nrcan.gc.ca/recent/2015/index-en.php (last accessed 15 February 2017), respectively. Strong-motion recordings were obtained from the BC Smart Infrastructure Monitoring System (BCSIMS) developed by Dr. Carlos Ventura (University of British Columbia). The BCSIMS strong-motion network is operated and maintained by Natural Resources Canada (Geological Survey of Canada) and BC Ministry of Transportation and Infrastructure.

2.6. Acknowledgements

2.7. References

Beyreuther, M., Barsch, R., Krischer, L., Megies, T., Behr, Y., & Wassermann, J. (2010). ObsPy: A Python Toolbox for Seismology. *Seismological Research Letters*, *81*(3), 530–533. http://doi.org/10.1785/gssrl.81.3.530

Bonilla, L. F., Steidl, J. H., Gariel, J. C., & Archuleta, R. J. (2002). Borehole response studies at the Garner Valley Downhole Array, Southern California. *Bulletin of the Seismological Society of America*, *92*(8), 3165–3179. http://doi.org/10.1785/0120010235

Britton, J. R., Harris, J. B., Hunter, J. A., & Luternauer, J. L. (1995). The bedrock surface beneath the Fraser River delta in British Columbia based on seismic measurements. *Current Research*, *83–89*.

Cassidy, J. F., & Rogers, G. C. (1999). Seismic site response in the greater Vancouver, British Columbia, area: Spectral ratios from moderate earthquakes. *Canadian Geotechnical Journal*, *36*(2), 195–209. http://doi.org/10.1139/cgj-36-2-195

Cassidy, J. F., & Rogers, G. C. (2004). Variation in ground shaking on the Fraser River delta (Greater Vancouver , Canada) from analysis of moderate earthquakes. In *13th World Conference on Earthquake Engineering* (p. 7).

Hunter, J. A., & Christian, H. A. (2001). Use of Shear Wave Velocities to Estimate Thick Soil Amplification Effects in the Fraser River Delta, British Columbia. *Symposium on the Application of Geophysics to Engineering and Environmental Problems 2001*, (March), SSI1-SSI1. http://doi.org/10.4133/1.2922943

Hunter, J. A., Dallimore, S., & Christian, H. (1997). Borehole measurements of shear wave velocity discontinuities in Quaternary sediments, Fraser River delta, British Columbia. *Current Research 1997-A, Geological Survey of Canada*.

Hunter, J. A., Douma, M., Burns, R. A., Good, R. L., Pullan, S. E., Harris, J. B., Luternauer, J. L., & Best, M. E. (1998). Testing and application of near-surface geophysical techniques for earthquake hazards studies, Fraser River delta, British Columbia. *Bulletin of the Geological Survey of Canada*, (525), 123–145.

Konno, K., & Ohmachi, T. (1998). Ground-motion characteristics estimated from spectral ratio between horizontal and vertical components of microtremor. *Bulletin of the Seismological Society of America*, *88*(1), 228–241.

Molnar, S., & Cassidy, J. F. (2006). A Comparison of Site Response Techniques Using Weak-Motion Earthquakes and Microtremors. *Earthquake Spectra*, *Vol. 22*(1), 169–188.

Molnar, S., Cassidy, J. F., & Dosso, S. E. (2004). Site response in Victoria, British Columbia, from spectral ratios and 1D modeling. *Bulletin of the Seismological Society of America*, *94*(3), 1109–1124. http://doi.org/10.1785/0120030195

Molnar, S., Cassidy, J. F., Monahan, P. A., & Dosso, S. E. (2007). Comparison of geophysical shear-wave velocity methods. *9th Canadian Conference on Earthquake Engineering*, (June), 390–400. http://doi.org/10.4095/222259

Molnar, S., Cassidy, J. F., Olsen, K. B., Dosso, S. E., & He, J. (2014a). Earthquake ground motion and 3D Georgia basin amplification in Southwest British Columbia: Deep Juan de Fuca Plate scenario earthquakes. *Bulletin of the Seismological Society of America*, *104*(1), 301–320. http://doi.org/10.1785/0120110277

Molnar, S., Cassidy, J. F., Olsen, K. B., Dosso, S. E., & He, J. (2014b). Earthquake Ground Motion and 3D Georgia Basin Amplification in Southwest British Columbia: Shallow Blind-Thrust Scenario Earthquakes. *Bulletin of the Seismological Society of America*, *104*(1), 321–335. http://doi.org/10.1785/0120130116

Molnar, S., Dosso, S. E., & Cassidy, J. F. (2013). Uncertainty of linear earthquake site amplification via Bayesian inversion of surface seismic data. *Geophysics*, *78*(3), WB37-WB48.

Monahan, P. A. (2005). Soil hazard map of the lower mainland of British Columbia for assessing the earthquake hazard due to lateral ground shaking. *9th Canadian Conference on Earthquake Engineering*.

Monahan, P. A., & Levson, V. M. (1997). Earthquake hazard assessment in greater Victoria, British Columbia: Development of a shear-wave velocity model for the Quaternary deposits. *Geological Fieldwork*, *1996*(1), 467–479.

Monahan, P. A., & Levson, V. M. (2000). Quaternary Geological Map of Greater Victoria, British Columbia. *Geological Survey, Ministry of Energy and Mines, Victoria, B.C., Geoscience Map 2000*, *2*.

Monahan, P. A., Levson, V. M., Henderson, P., & Sy, A. (2000). Relative amplification

of ground motion hazard map of Greater Victoria. *British Columbia Geological Survey, Ministry of Energy and Mines, Victoria, BC, Geoscience Map*, *3*.

NBCC, A. (2005). National Building Code of Canada. *Institute for Research in Construction*.

Onur, T., Molnar, S., Cassidy, J., Ventura, C., & Hao, K. X. S. (2004). Estimating site periods in Vancouver and Victoria, British Columbia using microtremor measurements and SHAKE analyses. *Canadian Geotechnical Conference, Quebec City, Quebec*, 24–27.

Ventura, C., Turek, M. E., Johanssen, K., Kaya, Y., Yao, F., & Sothby, B. (2016). British Columbia Earthquake Early Warning System. *Proceedings of 16th World Conference of Earthquake Engineering, Santiago, Chile, January 9-13 2016*.

Chapter 3

3. Application of passive seismic methods at 13 school sites to improve earthquake site assessment in the Greater Vancouver region

3.1. Introduction

3.1.1. Earthquake site classification

Local geology is well known to have a large influence on observed earthquake ground motion. The upper hundreds of meters to kilometres of material at a site alters ground shaking based on variation in seismic impedance. For example, 1D site effects would include amplification from the typical decrease in impedance towards surface and from resonance within layers. 3D site effects include basin and topographic (resonance) effects from variation in impedance between boundaries or surfaces. Predicting site effects is thus very important in seismic hazard analysis. In particular, V_S of a material is directly related to the stiffness, and so is a key property for evaluating site response.

First introduced by Borcherdt (1994), the time-averaged V_S to a depth of 30 meters (V_{S30}) is widely used as a simple, unambiguous and easily obtained parameter for site classification (Boore et al., 2011), that relates the behaviour of soil to the average stiffness of the site. V_{S30} is calculated as 30 m divided by the sum of shear wave travel times of each layer with thickness h,

$$V_{S30} = \frac{30}{\sum(h/V_S)}. \tag{3.1}$$

V_{S30} is a simplified predictor of earthquake site response and ubiquitous in seismic hazard analysis including ground-motion prediction equations (GMPEs) and building codes worldwide. In Canada, seismic design provisions of the National Building Code of Canada (NBCC) and Canadian Highway and Bridge Design Code (CHBDC) adopted the use of V_{S30} for earthquake site classification in 2000 and 2015, respectively. Table 1.1 provides the V_{S30} boundaries for each NBCC and CHBDC earthquake site class.

The preferred method for obtaining V_{S30} is a site-specific measurement (Wair et al., 2012), such as using invasive borehole techniques (e.g. downhole and crosshole), or non-invasive seismic techniques. Borehole techniques are not effective at the large spatial scales needed for urban or regional microzonation due to time and cost limitations, so non-invasive surface-based seismic techniques are a practical alternative.

Surface seismic techniques are broadly divided into two categories: active or passive source. Active source techniques involve manual generation of energy, such as from a hammer hitting a plate or an explosive. However active-source methods are often ill suited for urban applications, which are often areas where accurate hazard analysis is imperative due to the high associated seismic risk. For example, explosives and generators for mechanical sources can cause public disturbance, long array lengths potentially conflict with street design, and body-wave methods fundamentally cannot cope with common velocity inversions found in urban environments (e.g. sewers, tunnels, basements). Active source surface wave analysis such as Spectral Analysis of Surface Waves (SASW; Stokoe et al., 1988) and Multichannel Analysis of Surface Waves (MASW; Park et al., 1999) are also limited by the frequency content of the source, typically resulting in a shallow depth of investigation (tens of meters).

Passive source techniques instead use background seismic energy, known as ambient vibrations or microtremor. This seismic energy originates from various natural processes including tides, ocean waves and wind at frequencies < ~1 Hz, as well as from human activity at frequencies > ~1 Hz. A major advantage of passive seismic methods is a wider source frequency band than a common active source (Wathelet, 2005), which allows sampling of a large range of depths. Hence, analysis of these vibrations can reveal useful information about the near surface without the need for large arrays and invasive measurements, and so passive methods are gaining significant popularity as inexpensive, rapid and non-invasive methods.

Passive seismic techniques for retrieving near surface impedance information (i.e., V_S depth profiling) were first established by Aki (1957), who developed a passive survey method involving a two-dimensional (2D) array such as a triangle or circle to record

ambient surface waves. Passive methods were further developed by others: Asten & Henstridge (1984) processed ambient noise recorded by seven seismometers in a cross-shaped array with a radius of several kilometers. Ambient vibrations are widely used in global seismology to obtain the velocity structure of the Earth's crust. Passive techniques are not without their disadvantages. The ambient wavefield is typically assumed to consist primarily of surface waves (Arai & Tokimatsu, 2004) and the resolution of these methods is therefore limited by the depth penetration of surface waves, which ranges from tens to hundreds of metres depending on array aperture and wavefield-frequency content. In addition, the assumption of a spatially random ambient wavefield may be incorrect when vibrations are directionally biased by cultural activities.

3.1.2. Proxy methods for V_{S30}

For regional microzonation studies, obtaining a high-resolution map of predicted site response (e.g., V_{S30}) is difficult due to logistical and cost issues of traditional site-specific V_S-profiling methods on a large scale and in urban environments. In this case there are various alternative methods to rapidly approximate V_{S30} that warrant comparison.

Site classification mapping can be performed on a large scale using a well-known property of the region as a proxy for V_{S30}, such as using surficial geology (e.g. Tinsley and Fumal, 1985; Park and Elrick, 1998), or using topographic slope (Wald and Allen, 2007). In general these methods are subject to high uncertainty, as they do not consider subsurface impedance contrasts. Thompson et al. (2014) were successful in the integration of topographic data with geology and site-specific measurements for California, but found the map uncertainty to be significantly reduced in areas of denser site-specific measurements. Therefore site-specific measurement is an important part of V_{S30} mapping, even if used in combination with lower-resolution proxy methods.

3.1.3. Aims and objectives

In this chapter, we perform we perform site-specific ambient vibration analyses at 13 school sites in southwest BC, Canada. We record ambient vibrations at 11 high-priority seismic risk schools (Figure 3.1) of the BC school seismic retrofit program as well as 2

schools with strong-motion instrumentation of an earthquake early warning network (Ventura et al., 2017). The majority of these sites are in Greater Vancouver, with two sites further east in the Fraser Valley (Abbotsford and Hope), and a single school on southern Vancouver Island (Colwood). Important parameters that govern site response, e.g., V_S profile(s), fundamental peak frequencies, depths of significant impedance contrasts, are retrieved from Microtremor HVSR (MHVSR) and surface wave dispersion analyses of the passive-seismic recordings. We provide geological interpretation of the retrieved V_S estimates in conjunction with nearby stratigraphic profiles when available, as well as compare with previous limited V_S estimates of geologic units in the region. We evaluate our earthquake site classifications (V_{S30}) based on site-specific *in situ* V_S measurements with previous classifications based on V_S proxies including mapped Quaternary geology and topographic slope. The presented case studies are a notable contribution to public earthquake site assessments in the Vancouver region. This study is a continuation of passive-seismic site characterization case studies in BC (Molnar et al., 2010; Molnar et al., 2013; Molnar et al., 2014) which serve as the basis for an initiated 5-year seismic microzonation effort in the region.
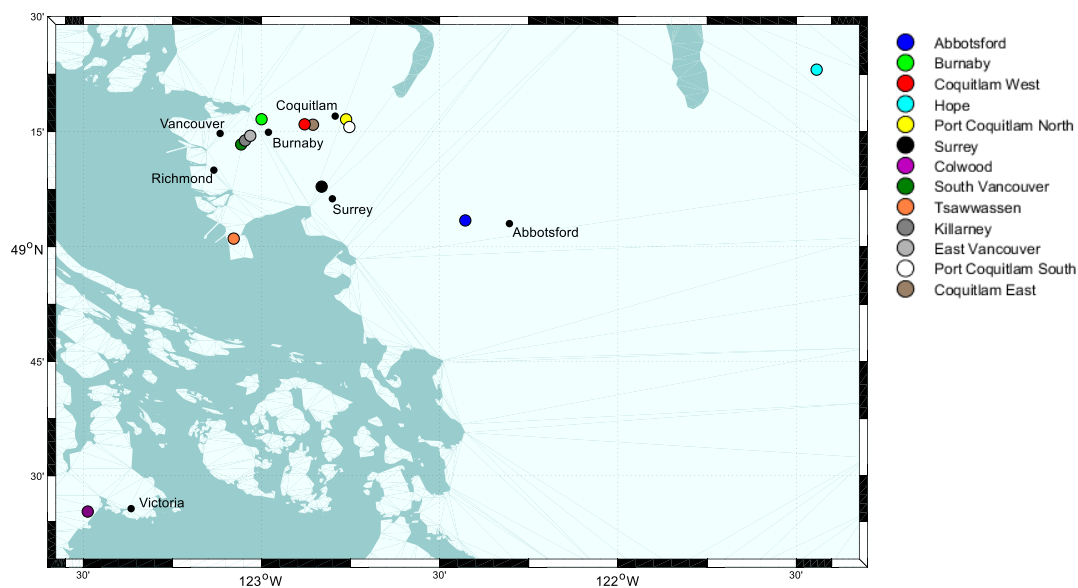
Figure 3.1. Locations of 13 school sites (filled circles) in southwest BC. Major urban centres are labelled and marked by small black circles.

3.2. Geological Setting and Previous Site Classifications

The bedrock in the Greater Vancouver region consists of Tertiary sandstone, mudstone and conglomerates. This is generally buried under more recent sediments to depths of up to 800 m at Ladner (Britton et al., 1995). The overburden is much shallower in the north, and bedrock is exposed in outcrops in Vancouver and the Stanley Park sea cliffs. The V_S of this bedrock ranges from around 2 to 3.5 km/s (Monahan and Levson, 2000). Compact Pleistocene deposits overlie this bedrock over much of the Greater Vancouver area. These fine sands and silts of glacial and interglacial origin have an average V_S that varies from 0.4-1.1 km/s (Hunter & Christian, 2001). The Ice-age sediments are buried in the Fraser delta by thick unconsolidated Holocene sediments. These silts, sands and clays are seismically soft (average V_S between 200-300 m/s [Hunter et al., 1998]), and reach thicknesses of 300 m in the centre of the delta (Hunter et al., 1997). Thus we expect significant impedance contrasts at both the Holocene-Pleistocene and Pleistocene-Tertiary geologic boundaries.

We investigate the mapped geology at the 10 school sites that are in Greater Vancouver. GeoMap Vancouver (Turner et al. 1997) is a compilation of previous geological mapping in the region. Figure 3.2 presents the GeoMap Vancouver geologic units, where geology is differentiated into lowland (Holocene sediments), upland (Pleistocene sediments) and Tertiary bedrock. Most of our stations in the Greater Vancouver region occur on upland or Pleistocene sediments, apart from Killarney and Port Coquitlam South (both on lowland sediments). Outside of Greater Vancouver (not shown in Figure 3.2, see Figure 3.1), the site at Abbotsford is on upland silt and clay, the Colwood site sits on the sand and gravel of the Colwood delta (Monahan & Levson, 2000a), and the Hope site sits on thick Fraser River fluvial deposits (Monger & Lear, 1989). A compilation of 60 stratigraphic depth profiles from both boreholes and outcrops (relevant locations plotted as black squares in Figure 3.2) and interpreted cross-sections in the Fraser Lowlands was published by Armstrong (1984) and illustrates the varying thickness of the Quaternary geology of the area.
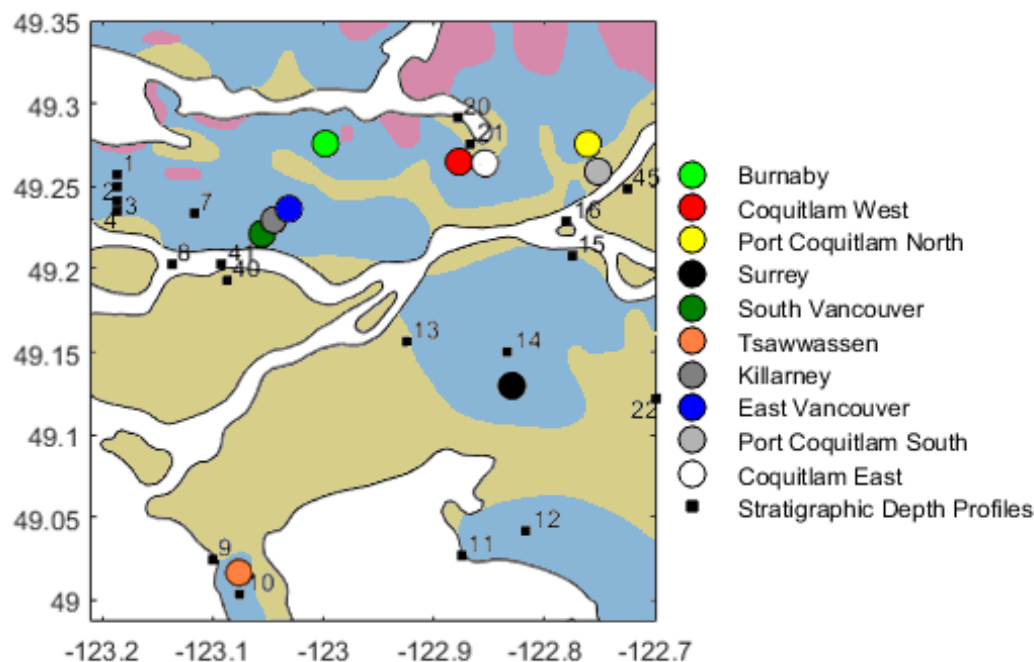
Figure 3.2. School site locations in Greater Vancouver denoted by filled circles. Locations of relevant stratigraphic profiles are shown by numbered squares, which are detailed in Armstrong (1984). Background map shading exhibits simplified geology (Turner et al., 1997); lowland (Holocene) sediment shown in beige, uplands (Pleistocene) sediment shown in blue, and Tertiary bedrock shown in pink.

There are few sources of publicly available shear-wave velocity measurements in the region. Hunter et al. (1998) is a GSC compilation of ~500 V_S profiles from downhole, seismic cone penetration testing, seismic refraction and spectral analysis of surface waves (SASW) methods limited to the Fraser River. The soft lowland sediments of the Fraser delta are widely recognized as prone to high amplification and liquefaction potential (e.g. Cassidy & Rogers, 2004) due to their thickness and relatively low seismic velocity (Monahan et al., 1993; Hunter et al., 1998). Figure 3.3a shows an interpolated map of earthquake site class (Hunter and Christian, 2001) based on the V_{S30} measurements across the Fraser River delta.

Monahan and Levson (2001) supplemented the Hunter et al. (1998) dataset with an additional 20 sites in Chilliwack (Fraser Lowland) and 19 sites in the Victoria area (Vancouver Island) to develop a shear-wave velocity model of near-surface deposits of

southwest BC. The V_S model consists of average V_S estimates for the upper 20 m, 30 m, or full depth of mapped Quaternary geologic units. The sparsely derived V_{S30} model is combined with mapped Quaternary geology to generate amplification hazard maps for Greater Victoria (Monahan and Levson, 2000) and Greater Vancouver (Monahan, 2005), which is shown in Figure 3.3b. The variable V_S within each of the three major geologic units in Greater Vancouver combined with variable depth of each unit leads to the full range of site classes present across the region.

Figure 3.3c displays site class mapping from proxy-V_{S30} estimates of the USGS global V_{S30} model based on topographic slope (Allen and Wald, 2009). Pixelation results from resolution of the original digital elevation model (DEM). Figure 3.3b and c are largely similar. A wide range of site classes (V_{S30}) are observed from class AB through to class E across the region, as well as a "bi-modal" stiffer class C conditions for upland areas compared to softer classes D-E for the lowland Fraser River delta. Site classification mapping from dense V_{S30} measurements for the Fraser River delta (Figure 3.3a) varies between classes D and E too; however, the location or boundaries of class D and E zones is not similar to Figure 3.3b based on geology or Fig. 3c based on topographic slope.
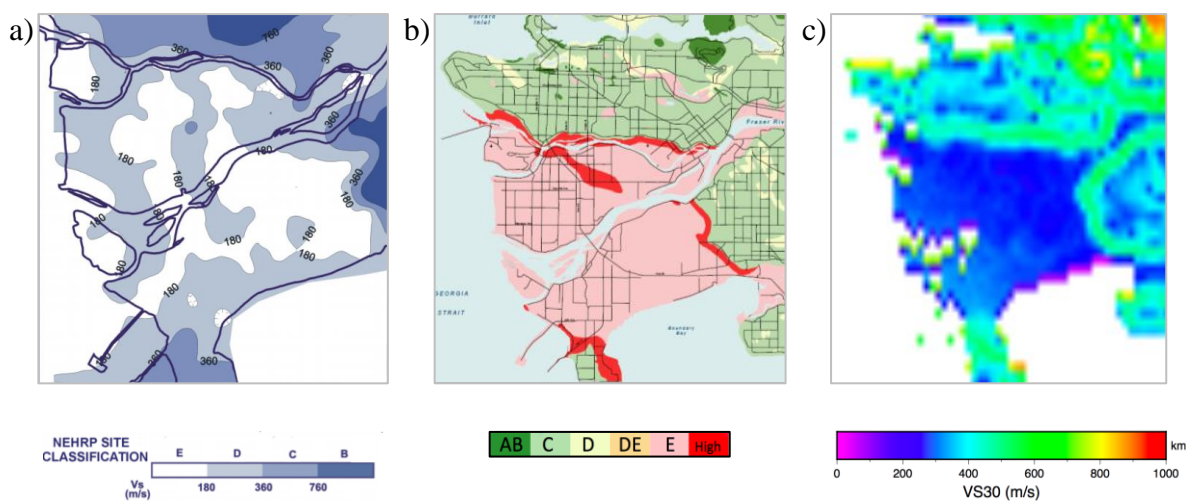
Figure 3.3. Site classification maps from (a) V_S data (modified from Hunter and Christian, 2001), (b) sparse V_S data combined with Quaternary mapping (modified from Monahan, 2005), and (c) proxy-V_{S30} estimates based on topographic slope (Allen and Wald, 2009).

The need for published V_S profiling case studies to compile a robust V_S database for the region is readily apparent from the discrepancy between mapped classes based on V_S data (Figure 3.3a) compared to proxy information (Figure 3.3b and c). Surficial trends cannot capture variations in the underlying Pleistocene and Tertiary bedrock surfaces.

3.3. Theoretical Background

Measurement of ambient vibrations for V_S profiles generally involves either a single station (HVSR analysis) or several stations in an array (surface wave dispersion analysis). These single and multi-station methods are often used in combination, and because both methods are a measure of subsurface elastic properties, they can both be used to retrieve a V_S profile using an inversion algorithm.

3.3.1. Single station HVSR

HVSR analysis involves calculating the spectral ratio between the horizontal and vertical components of a seismic record (Nakamura, 1989; Nogoshi & Igarashi, 1971), and only requires a single three-component seismometer. Hence, HVSRs are relatively fast to obtain. HVSR analysis in this paper is performed using microtremor records (MHVSR), but the technique is also commonly performed for earthquake data (Earthquake HVSR; EHVSR).

A HVSR typically displays a peak frequency (f_{peak}) that matches the fundamental frequency (f_0) of the site:

$$f_0 = \frac{V_{S\ Ave}}{4h},\tag{3.2}$$

where V_{Save} is the soil average V_S and h is soil thickness (Haskell, 1960; Kramer, 1996). (3.2 says that for a single soil layer over an elastic half-space, vertical (1D) SH-wave propagation may become trapped or resonant within the soil layer dependent on its average V_S and thickness. The value of f_0 is an important parameter in site classification, as it describes the frequency at which shaking amplitude is typically highest.

The microtremor wavefield is typically assumed to be primarily comprised of surface waves (e.g. Bonnefoy-Claudet et al., 2008). When there is a strong impedance contrast at

depth in a layered medium, the MHVSR is an approximation of the Rayleigh wave ellipticity (Scherbaum et al., 2003).

3.3.2. Surface wave array methods

Surface wave array techniques use the dispersive property of surface waves, which describes how waves of longer wavelengths penetrate to greater depths and pass through higher velocity layers, so arrive earlier than waves in shallow lower velocity material. Thus by measuring Rayleigh wave phase velocity as a function of frequency, known as a dispersion curve, we can obtain information on subsurface elastic material properties (velocity, density, and layer thickness) via inversion.

Active-source surface wave methods use seismic sources similar to body wave methods (e.g. hammer and plate, explosives), whereas passive-source methods use the ambient wavefield under the assumption that it is dominated by surface waves at distances larger than one wavelength from the sources (Arai and Tokimatsu, 2004). In comparison to active surface wave methods (MASW, SASW) where there is a known direction of source wave propagation, the ambient wavefield is generally random, so passive recording requires sensors in a geometric array which is roughly circular to ensure equal recording of all azimuths (Wathelet, 2005). By expanding the radii of a geometric array, sampling of greater depths is achieved, as lower frequency surface waves can be recorded.

Surface wave phase velocities are commonly extracted from the ambient vibration recordings using either frequency wavenumber (FK; Lacoss et al., 1969) or spatial autocorrelation (SPAC; Aki, 1957) analysis. The FK technique involves calculating a 2-dimensional power spectral density for the slowness (1 / velocity) vector of an incoming wave. For a given frequency, the maximum semblance (coherence of the data) of the spectra gives the best estimate of velocity and azimuth, and the final dispersion is the summation of all azimuths. The High Resolution Frequency Wavenumber method (HRFK; Capon, 1969) additionally amplifies the coherent signal amongst array recordings compared to the FK method.

SPAC processing for the extraction of ambient array-based surface wave dispersion was first proposed by Aki (1957), and assumes that the wavefield is stochastic and stationary in space and time. This means that the method requires a simple layered earth, and is most accurate when energy does not have a directional bias. This method is thus well suited to urban environments where ambient vibration comes from a variety of sources and azimuths. For an array of sensors at varying azimuths, the coherency spectra of the vertical component recordings between all pairs across the array are determined, which indicates the similarities between the recordings as a function of frequency. For two signals $v_0(t)$ and $v_\xi(t)$ recorded for time t at stations separated by distance ξ, the autocorrelation coherency spectrum is given by:

$$\phi(\xi) = \frac{1}{t} \int_0^t v_0(t)\, v_\xi(t)\,.$$

(3.3)

The coherency spectra for all pairs in the array are then averaged over each azimuth according to the interstation separation, resulting in spatially averaged coherency spectra, known as SPAC coefficients. For a Rayleigh wave recorded by vertical components filtered about frequency ω, the SPAC coefficient $\overline{\rho_z}(r, \omega)$ is given by:

$$\overline{\rho_z}(r, \omega) = J_0\left(\frac{\omega r}{c_R(\omega)}\right),$$

(3.4)

where $c_R(\omega)$ is the phase velocity of the dispersive Rayleigh waves as a function of frequency, r is the interstation distance, and $J_0(x)$ is the Bessel function of zero order, defined by:

$$J_0(x) = \frac{1}{\pi} \int_0^\pi \cos\big(x \cos(\varphi)\big)\, d\varphi,$$

(3.5)

where φ is interstation azimuth and x is propagation direction. Using Equation 3.4 the phase velocity is found at each select frequency for every pair, and these phase velocities are complied into histograms that indicate the dispersion trend of the site, which can be picked manually or found using grid search algorithms. By expanding the array and repeating the measurements and coherency calculations, each array radii provides coherency spectra with different frequency-bandwidth information, so combining the spectra from all arrays makes up the full dispersion curve of the site. The Modified

Spatial Auto Correlation method (MSPAC; Bettig et al., 2001) is a modified SPAC technique to correct for non-circular arrays.

Asten and Henstridge (1984) found that to obtain reliable dispersion estimates the size of the array should be larger than the longest wavelength of interest, and the station spacing less than half the shortest wavelength of interest. The array geometry (size, shape, number of sensors) directly impacts the resolution limit (k_{min}) and spatial aliasing limit (k_{max}) of the array, which define a frequency bandwidth region within which dispersion estimates are reliable (Tokimatsu, 1997). The resolution depth of surface wave dispersion methods is also limited by f_{peak} in practice. Vertical-component recordings typically lose significant energy content at f_{peak} (most energy is due to horizontal motion at f_{peak}) and dispersion estimates are limited to frequencies higher than f_{peak} (Scherbaum et al., 2003).

Like all surface wave techniques, array methods are limited by a shallow depth of investigation (approximately one-half of the wavelength for a Rayleigh wave; Wightman et al, 2003). Molnar et al. (2010) demonstrate reliable V_S profiling is achieved to ~110 m depth on the Fraser River delta from passive-source dispersion data in comparison to downhole V_S measurements to 300-m depth. Surface wave array techniques lose resolution with depth and V_S of the modelled elastic half-space (i.e., bedrock) is rarely constrained (Bonnefoy-Claudet et al., 2006). Because the data is averaged spatially across the array the resulting geometry is inherently 1D, meaning that the array technique is not suitable for sites with strong lateral variations.

3.4. Passive Seismic Recordings

3.4.1. Data collection

Microtremor recordings are collected using MoHo s.r.l. Trominos®, which have three-component high-sensitivity velocimetric channels and a low frequency limit of 0.1 Hz. At each site, up to 9 Tromino® instruments are arranged in symmetric cross- or circle-shaped arrays with a central sensor (e.g. Figure 3.4).
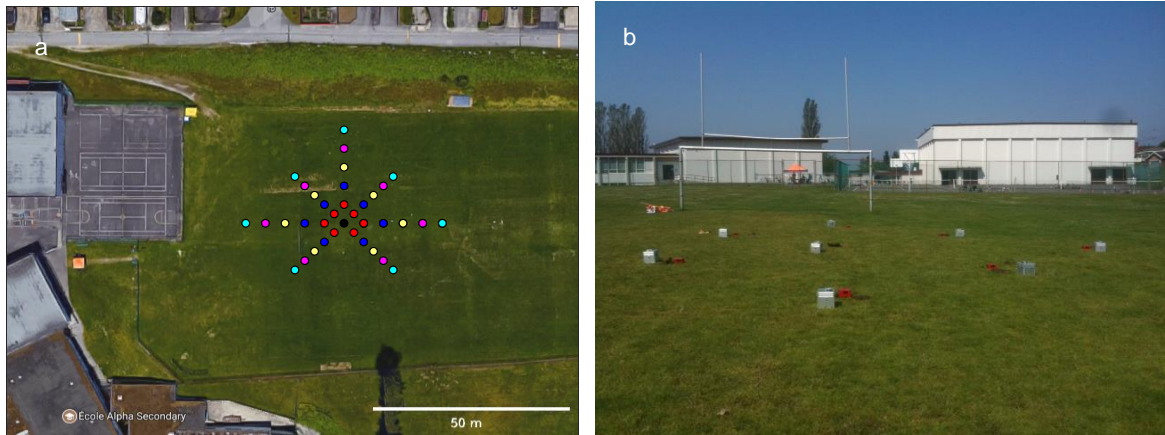
Figure 3.4. (a) Overview map of 8-sensor acquisition arrays at Burnaby (modified from Google Maps, 2017). Each circle denotes the location of a Tromino® microtremor recording, coloured by each array radius, ranging from 5 to 25 m. (b) Photo of 5-m array at Burnaby (Photo credit Sheri Molnar).

Table 3.1 details the array acquisition geometries, which are related to the depth penetration and resolution of each array radius. The appropriate array geometry is selected or altered depending on the physical limitations of each site. Sensors are set to record simultaneously for 15-20 minutes at a sample rate of 128 Hz. The array is successively expanded (or reduced) about a central sensor from a minimum radius of 5 m to a maximum of 50 m to sample greater depths and obtain the full dispersion characteristics of the site.

Table 3.1. Details of array geometry.

Site Location	Lat. (°N)	Long. (°E)	# of Sensors	Radius range (m)
Abbotsford	49.05	-122.42	7	5 - 25
Burnaby	49.27	-122.99	8	5 - 25
Coquitlam West	49.26	-122.87	7	5 - 30
Coquitlam East	49.264	-122.85	5	5 - 15
Hope	49.38	-121.44	7	10 - 50
Port Coquitlam North	49.27	-122.76	7	5 - 30
Port Coquitlam South	49.259	-122.75	5	5 - 15
Surrey	49.12	-122.82	6	5 - 40
Killarney	49.22	-123.04	9	5 - 25
Colwood	48.42	-123.48	7	5 - 35
South Vancouver	49.22	-123.05	9	5 - 25
Tsawwassen	49.01	-123.07	8	5 - 30
East Vancouver	49.24	-123.03	9	5 - 17

3.4.2. MHVSR analysis

Time-averaged MHVSRs from the full duration microtremor recording are calculated using open-source Geopsy software (version 2.10.1; Wathelet, 2017). For each location's three-component recording, time windows of 60 seconds are selected and a 5% cosine taper applied to each window. Some time windows contained unwanted 'noise' such as directional bias (e.g., people walking to/away from the sensor at the beginning/end of the recording) and are removed. The Fourier transform of each component is calculated using 100 logarithmically spaced frequency samples between 0.5 and 50 Hz and smoothed using a Konno and Ohmachi (1998) filter with a constant bandwidth of 40. The squared average of the two horizontal spectra is calculated and divided by the vertical spectrum to obtain the MHVSR curve.

Time-averaged MHVSR curves are calculated for all sensor locations of each array expansion stage, to confirm that the ratios did not vary significantly in space. If all or most time-averaged MHVSR curves are similar at the site of interest then the uniformity of subsurface ground conditions (a basic assumption for dispersion analysis) is confirmed. A single time-averaged MHVSR from a particular location (Figure 3.5) is

selected as representative of the site's subsurface ground conditions and used for subsequent inversion.
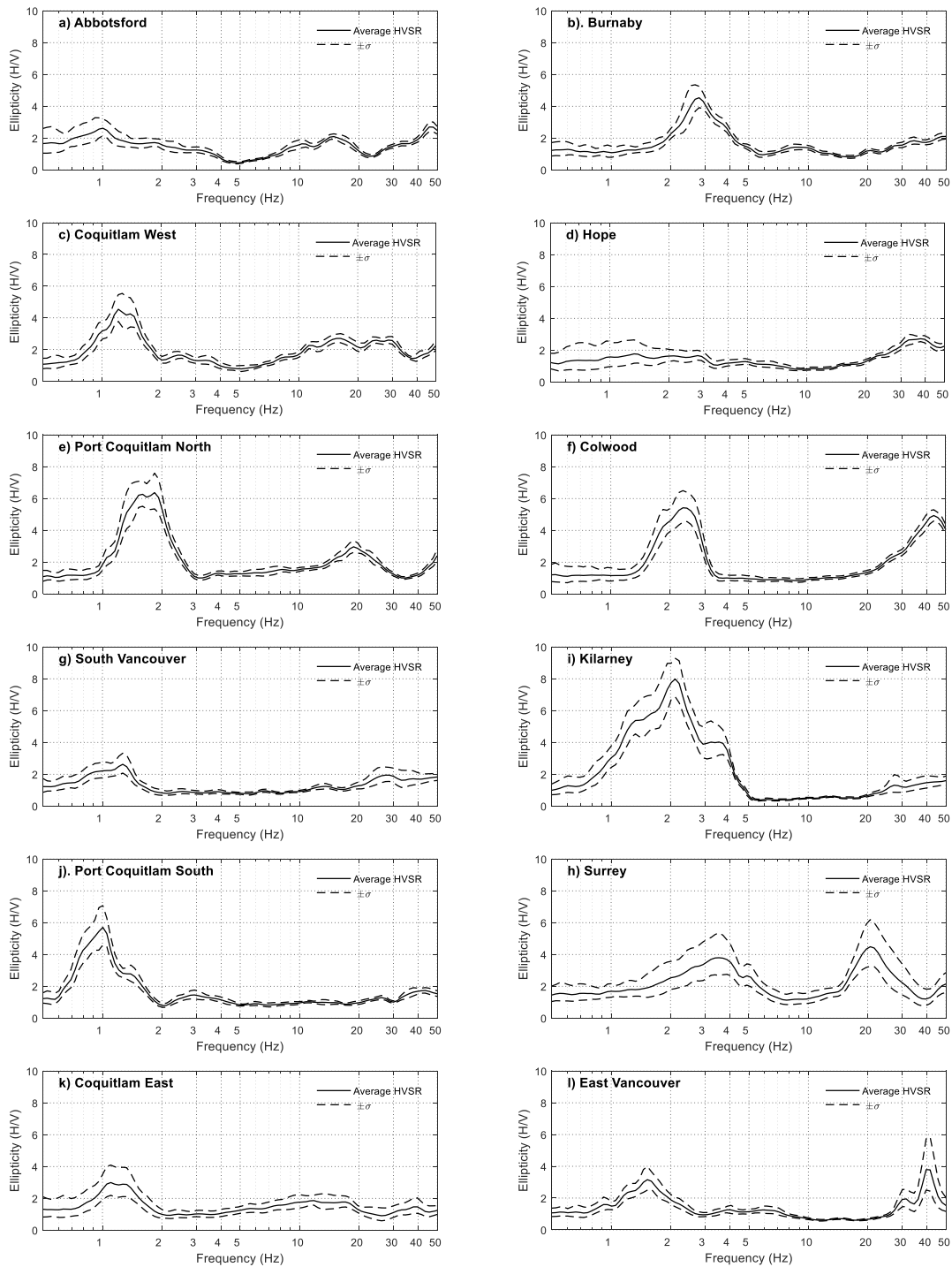
Figure 3.5. Time-averaged MHVSR curves representative for each site are shown with one standard deviation.

The time-averaged MHVSRs at each site (Figure 3.5) typically show a clear fundamental peak and provides confidence in reproducibility of the f_{peak} estimate. At 5 sites, the peak is less defined or of broad and low amplitude for Abbotsford, Hope, South Vancouver, Coquitlam East, and East Vancouver. At Tsawwassen (Figure A1 in Appendix), no significant peak is observed and the relatively flat MHVSR was rejected for inversion. A poorly defined peak could indicate that the 1D-layered assumption is not met and/or that the impedance contrast between layers is too low or too deep relative to the array setup and wavefield to generate notable amplification. However no peaks were so flat that no obvious peak was pickable when modifying the y-axis.

In general the MHVSRs display f_{peak} between 1 and 3 Hz. From 1D wave propagation theory (Equation 3.2) and roughly assuming an average V_S of 750 m/s (average V_S of Pleistocene deposits (Hunter & Christian, 2001) expected at upland sites), a 1 Hz peak corresponds to an impedance contrast at a depth of 190 m. Burnaby and Surrey show f_{peak} as high as 3 Hz, and correspond to a depth of around 60 m. If the average V_S is lower, than the estimated depth of a major impedance contrast will be shallower. Port Coquitlam North, Colwood, Surrey and East Vancouver clearly show additional peaks at higher frequencies (> 15 Hz), likely due to a shallow impedance contrast, suggesting an additional (assumed softer) upper layer. Secondary peaks at Colwood and East Vancouver are observed as high as 40 Hz.

3.4.3. Dispersion analysis

MSPAC (Bettig et al., 2001) dispersion analysis of array recordings is performed using Geopsy software (version 2.10.1; Wathelet, 2017). Wathelet et al (2008) found no significant difference between the FK and SPAC methods when determining a dispersion curve; however SPAC analysis generally provides a higher resolution dispersion curve over a larger frequency range (Zhao and Li, 2010). Each array's simultaneous vertical-component recordings are imported and the corresponding array geometry defined (Table 3.1). We assume, as is commonly done, that the vertical component recordings are dominated by Rayleigh surface waves. The MSPAC analysis implemented in Geopsy (Wathelet 2005) is accomplished here for each array radius using 50 logarithmically

sampled frequencies between 1 and 50 Hz. Fundamental-mode Rayleigh wave phase velocity estimates are manually picked at select frequencies from cumulative dispersion histograms from all arrays at each site. Quality control of dispersion picking is performed by considering the resolution (k_{min}) and aliasing (k_{max}) limit of each array, which also ensures the reproducibility of these results. The histograms together with the picked dispersion estimates (resampled logarithmically to a total of 50 points per curve) are shown in Figure 3.6. Most histograms show clear dispersion trends allowing simple picking. At some sites (Burnaby, Hope, Surrey), dispersion trends are poorly defined, resulting in dispersion picks over narrower frequency bandwidths. For the East Vancouver and Killarney sites, well-defined dispersion trends are not identified (see Appendix) and no dispersion curves are retrieved.

Using frequency as an inverse proxy of depth permits basic interpretation from the dispersion data. Most curves illustrate increasing phase velocities at lower frequencies (greater depth), as is generally expected. Velocities range from 200-850 m/s, with some stations showing a much wider range in phase velocities than others. The lowest phase velocities (softer soils) are observed at Abbotsford and Port Coquitlam South, whereas the highest velocities (stiffer soils) are observed at Burnaby, Hope and Surrey.
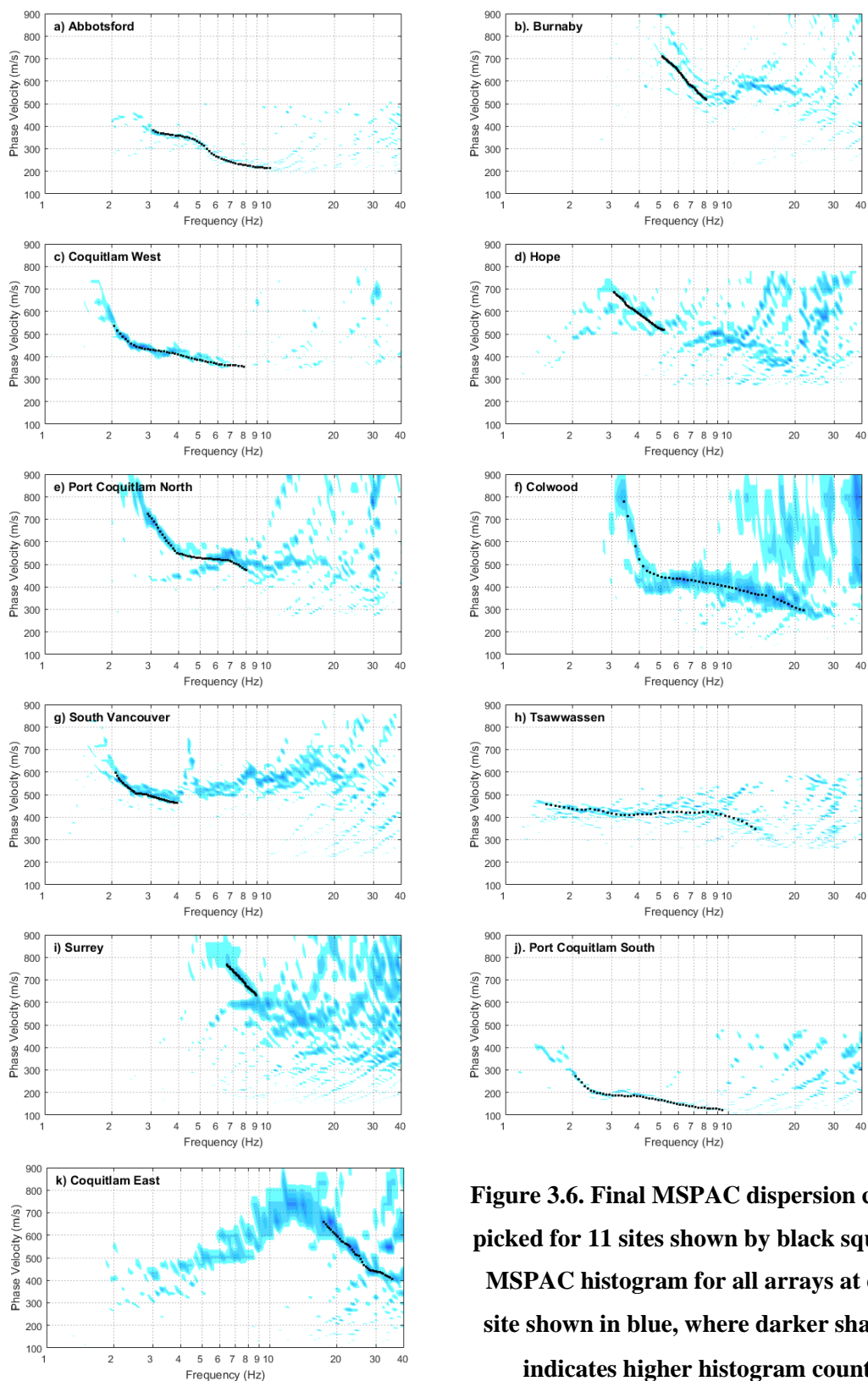
Figure 3.6. Final MSPAC dispersion curves picked for 11 sites shown by black squares. MSPAC histogram for all arrays at each site shown in blue, where darker shading indicates higher histogram count.

3.5. Inversion

The relationship between a system of parameters (*m*) and a set of observations of those parameters (*d*) is defined by:

$$d = G(m),$$

(3.6)

where *G* is the forward operator as a function of m that represents a physical process relating the two. The scientific process of inversion involves finding the model of physical parameters that replicate a set of observations, or in other words solving Equation 3.6 for *m*. If the relationship between parameters and observations is linear (e.g., d = G * m), the inverse problem can be solved simply using linear algebra (Tarantola, 1987). If there are more observations than parameters, then the inverse problem is generally well-posed, and a least squares method is commonly used (Tarantola, 1987). If there are more parameters than observations, the inverse problem is ill-posed, and there is an infinite number of solutions (Tarantola, 1987). This problem is called non-uniqueness, as there is no single unique solution that fits the observations. In most real life situations the relationship between the parameters and observations is non-linear, and there are many more parameters than observations. In these situations a complex iterative inversion algorithm is required to test the suitability of various models of parameter combinations to the observations.

A misfit function (*x*) describes the difference between the observations and the model. The inversion algorithm starts with an initial estimation of the model parameters, and iteratively alters the parameters to reduce the misfit function, i.e. "fit" the data. The inversion process effectively produces synthetic observations of the model, and attempts to match these to the real observations. Inversion techniques differ with how they iteratively choose parameters, as the exploration of the model space is often limited by the path taken.

Since Rayleigh wave ellipticity and dispersion curves are influenced by V_S structure, they can both be used to solve for V_S through inversion. The model that we are solving for is a layered earth model (each layer of thickness *h* is comprised of three elastic parameters:

compressional-wave velocity (V_P), V_S, and density) that agrees with or "fits" both the observed MHVSR and dispersion data. The first step of MHVSR and/or dispersion curve inversion involves a starting model input. The initial layered earth model parameterization is unknown; traditionally, many earth model parameterizations are tested (e.g., uniform, and linear or powerlaw gradients, over an elastic half-space; Molnar et al., 2010).

Dispersion curve inversion has historically been solved by linearized methods (aka derivative based) such as damped least squares (Herrmann, 1987). This involves linearizing the problem by calculating the partial derivative of the residuals, in order to minimize the misfit function. However these methods can get stuck in local minima for nonlinear problems (Herrmann, 1987). Recently as computational power has increased, non-linear direct search (derivative free) methods have emerged as efficient alternatives. These methods do not use the gradient of the misfit function and are well suited for non-linear problems. Instead direct search methods use pseudo-random Monte-Carlo sampling to search for misfit function minima, meaning they can also search the entire parameter space, avoiding local minima. These methods include uniform random search (Wiggins, 1969), simulated annealing (Rothman, 1985), genetic algorithms (Lomax & Snieder, 1994), and the neighbourhood algorithm (Sambridge et al., 1999) which is used in this study.

3.5.1. The neighbourhood algorithm

Like other direct-search methods, the neighbourhood algorithm involves stochastic sampling of a multidimensional parameter space. What makes the neighbourhood algorithm unique is that it uses the ensemble of misfit values (samples) from previous iterations to guide the next iteration by interpolating the misfit neighbourhood of samples using Voronoi cells (each cell is a region that is closer to a sample point than any other region). The number of samples can reach as high as tens of thousands, hence the need for computing power in direct-search methods. The Geopsy software package inversion routine, Dinver, uses a conditional neighbourhood algorithm (Wathelet, 2008). It has been modified from the original method to handle physical conditions (e.g. Poisson's

ratio) on the parameters to reduce model non-uniqueness and replotting of the misfit values (termed 'axis scaling') to optimize and thereby increase computational speed of the inversion.

The modified neighbourhood algorithm inversion process used in this study is described by Wathelet (2005, 2008), and briefly summarized here. First a set of models is randomly generated with a uniform probability from user-defined parameter distributions for a user-defined model parameterization (number of layers). The misfit function is calculated for these models, and the parameter space is split into Voronoi cells based on the location of these models. Then a specified number of lowest misfit cells are selected. A random walk is then performed, which is a sequence of perturbations to the model location along the axes. This defines the location of new models, which divides the parameter space into more Voronoi cells, and the process is repeated until a cell with a satisfactory misfit is obtained.

The misfit of the ellipticity curve considering the standard deviation of the peak is given by Equation 3.7 (Wathelet 2005):

$$misfit_{ellipticity} = \frac{(f_{peak})_{experimental} - (f_{peak})_{calculated}}{(df_{peak})_{experimental}}, \tag{3.7}$$

where $(df_{peak})_{experimental}$ is the standard deviation of the experimental peak frequency. The misfit between a synthetic dispersion curve and the measured curve is given by Equation 3.8 (Wathelet 2005):

$$misfit_{dispersion} = \sqrt{\sum_{i=1}^{n_F} \frac{(x_{di} - x_{ci})^2}{x_{di}^2 n_F}}, \tag{3.8}$$

where x_{di} is the velocity of the sample point at frequency f_i, x_{ci} is the velocity of the synthetic sample point at f_i, and n_F is the total number of samples considered.

3.5.2. Joint inversion implementation

Inversion of either dispersion or MHVSR data is non-unique; for example, fitting the peak frequency of MHVSR according to Equation 3.2 involves two opposing parameters (thickness and average velocity), which means that there is a trade off between them. As

in, for any given thickness, there are many solutions of the average velocity that will equally fit the MHVSR peak frequency, which makes the solution non-unique.

We reduce the non-uniqueness in this study by constraining the inversion process with both MHVSR and dispersion inputs simultaneously. This process is called joint inversion, and has been used to obtain V_S profiles in previous studies (e.g., Scherbaum et al. 2003, Parolai et al. 2005, and Arai and Tokimatsu 2005). Dispersion and MHVSRs are unique data sets, as they provide information over unique frequency bandwidths. Dispersion data occurs above f_{peak}, MHVSRs provides f_{peak} and frequencies below (Scherbaum et al., 2003). Additionally, MHVSR inversion is typically more sensitive to impedance contrast depth, whereas surface wave dispersion is more sensitive to velocities (Dal Moro, 2014). By inverting the two datasets together, they provide different parameter sensitivities and independently constrain different areas of the parameter space. We first invert each dataset separately to understand their respective contributions to the model, and then performed the joint inversion to find a model that best match both.

The lowest misfit solution is highly dependent on the starting parameterization of the model (i.e., depth discretization, parameter bounds), so it is very important that the model is geologically reasonable. We further reduce the amount of non-uniqueness by using *a priori* knowledge of the expected geology at the sites to affect the initial and on-going parameterization. First we assume that a one-dimensional Earth model is an accurate description of the sites, which assumes little lateral changes in layer thickness and velocities. By checking the similarity of the MHVSRs recorded in many locations at each site, we confirm that there is little lateral variation. The parameter bounds for each site are then constrained depending on each site's dispersion phase velocities and MHVSR characteristics, although they are generally kept to be reasonably wide, e.g. 0-100 m for the top layer thickness. In some cases known stratigraphy is also used to constrain the search limits for each parameter, e.g. limiting the first layer to a maximum of 500 m/s where we expect soft sediments at the surface, such as at Port Coquitlam South, Killarney, and Hope. We also obtain some basic estimates of parameters from the data; the dispersion curve gives an approximation of velocity extrema sampled by the Rayleigh waves, and the MHVSR f_{peak} provides a rough estimation of depth to the major

impedance contrast (Equation 3.2). Because density has minimal influence on dispersion, we fix this parameter at 2000 kg/m^3 for all layers. Poisson's ratio was used to link V_P to V_S for each layer sampled from a uniform distribution between 0.2 and 0.5.

To further address non-uniqueness, we apply the principle of Occam's Razor (simpler models are generally better) and attempt to keep the number of parameters as low as possible. However there has to be enough parameters to provide a suitable match to the complexity of the observations. Our solution is to start with a simple model (one uniform layer over a half-space), and progressively add layers until a sufficient fit was reached; the number of layers in the final model (including half-space) varies between 3 and 4 depending on the site. The robustness of the final results is also confirmed by running the same inversion multiple times using different random seeds to ensure that a similar result was obtained with different pseudo-random sampling.

Our goal in the inversion process is not to produce one best-fitting model, but a range of possible models that agree with the observations within an acceptable misfit. We increase the complexity of the earth model parameterization (i.e., added layers) until the 'misfit versus models generated' function levelled out and reached a minimum misfit indicating a sufficient number of parameters to adequately (and not over-) fit the data. We use the 1000 lowest misfit models, including the minimum misfit or optimal model, for interpretation.

3.6.　Retrieved V_S Profiles

Figure 3.7 shows the 1000 lowest misfit V_S profiles (models) that resulted from the inversion process, as well as the synthetic MHVSR and dispersion model predictions in comparison to the observations. How well the synthetic data agrees with the measured MHVSR and dispersion curves allows us to judge suitability of the V_S models, whereas the observed variability in the 1000 models allows us to identify model resolution and model parameter uncertainty. We note a full Monte-Carlo sampling routine without fixing model parameters is required to provide an unbiased sample of the model parameters (e.g., Molnar et al. 2010). Some disparity between the data and models is acceptable due to the inherent uncertainty in the data due to unwanted noise or human
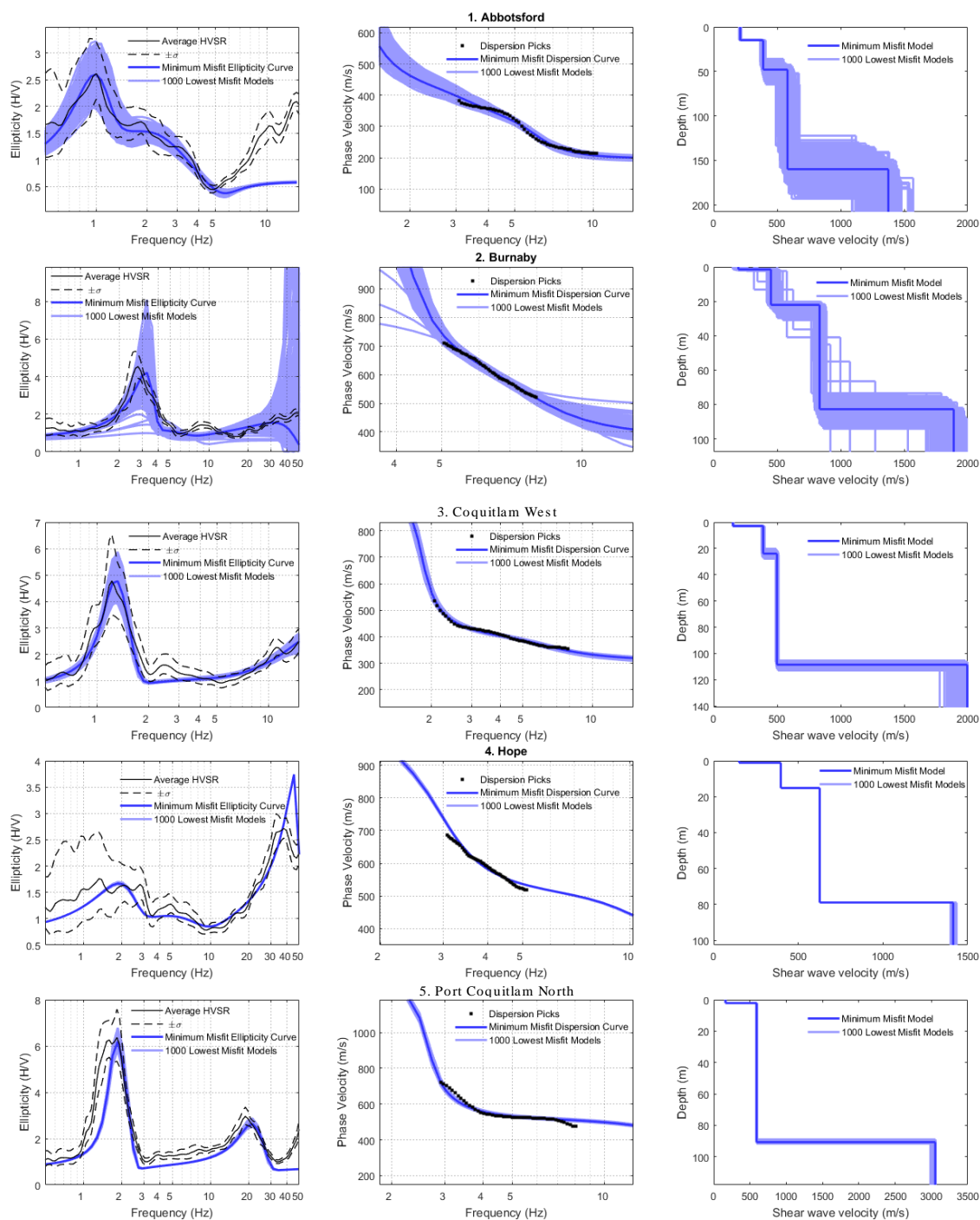
Figure 3.7. Panels from left to right for each site are average (black solid line) and one standard deviation (black dashed line) MHVSR and dispersion (squares) datasets, and inversion results shown as V$_S$ depth profiles (blue lines). Synthetic MHVSR and dispersion curves of the inverted models are shown in panels to the left with similar model shading.
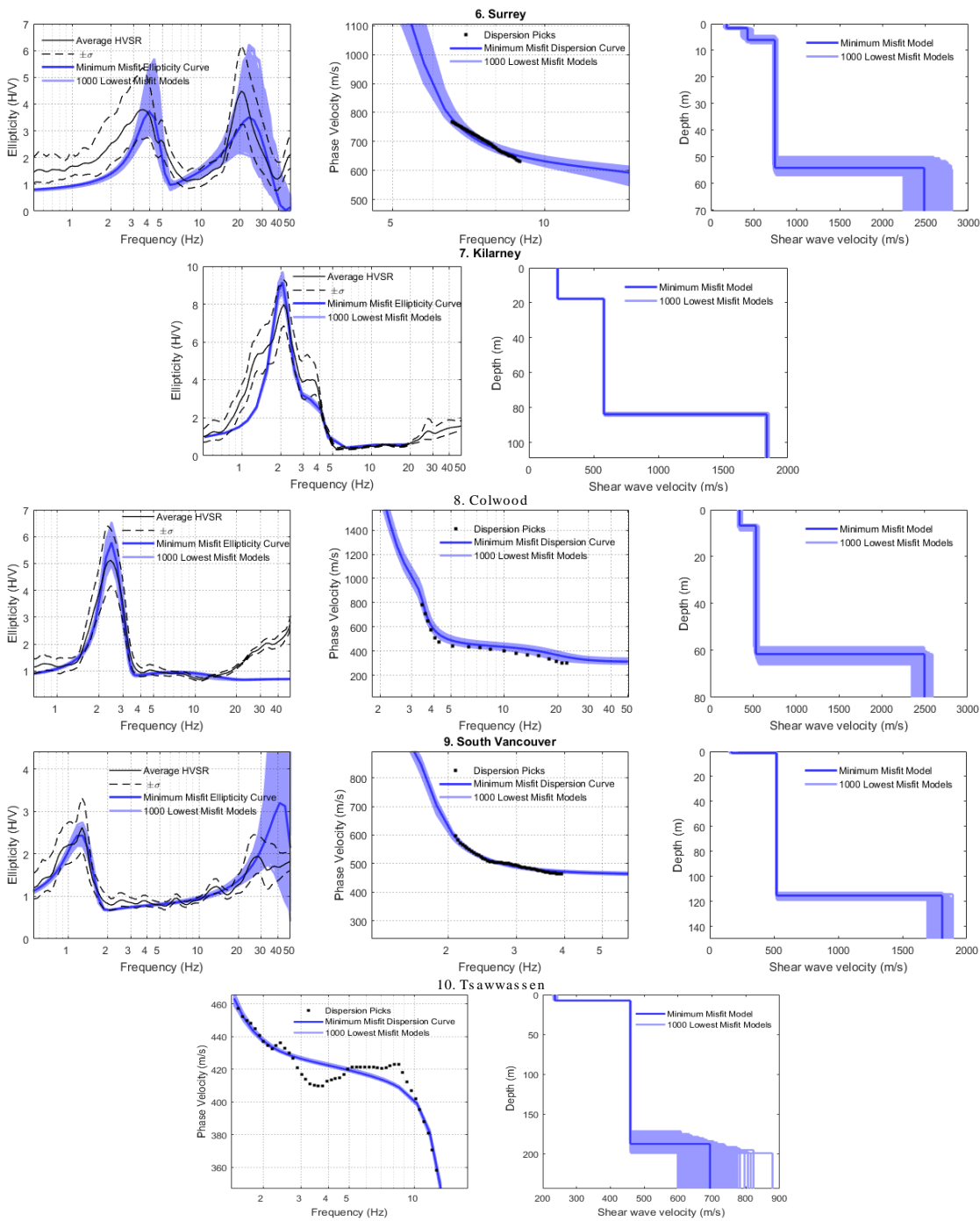
Figure 3.7. Continued.
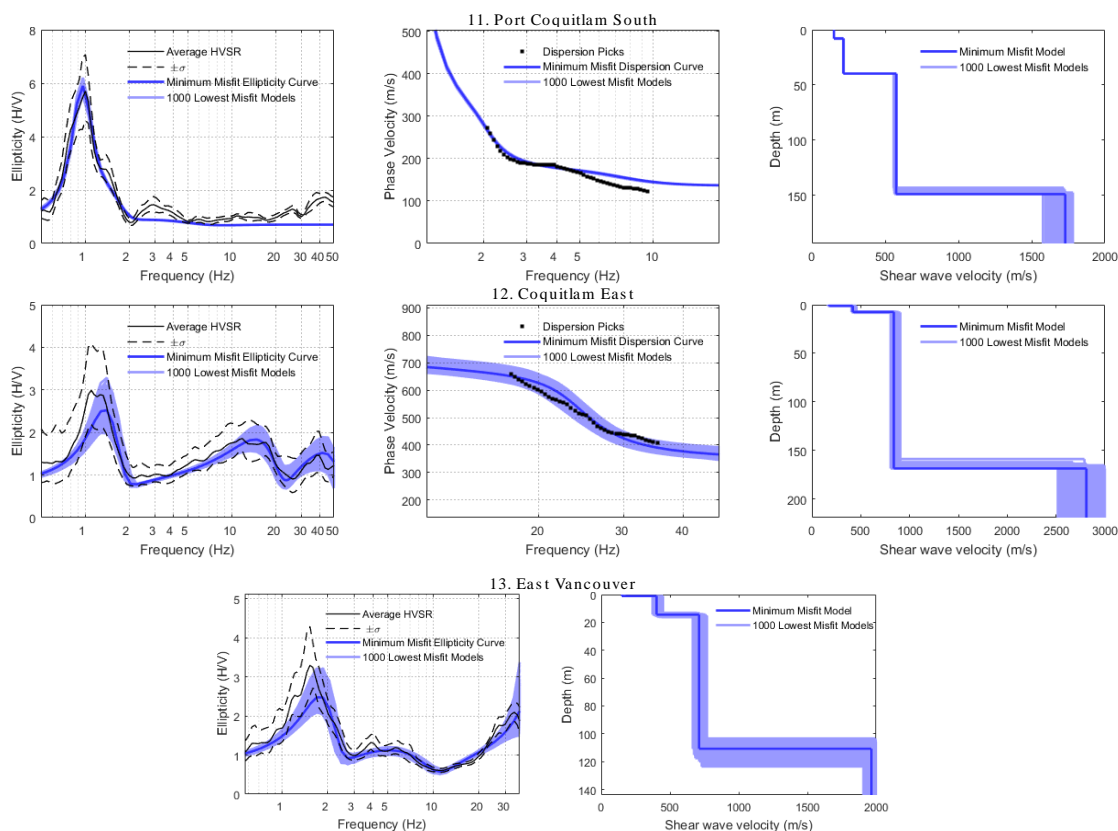
Figure 3.7. Continued.

error in picking. For this reason, it is also better to consider a range of values for each parameter shown by the variability in the 1000 models (although a slightly biased range) rather than a single 'best fit' model.

The joint inversion of MHVSR and dispersion data is generally successful. Fair agreement is obtained between the data and synthetics. The inversion results obtained are a balance of fitting both datasets equally; an equal fit of all MHVSR and dispersion estimates over the entire frequency bandwidth is rarely achieved. Abbotsford and Tsawwassen are the only sites where the fit is less ideal. At Abbotsford we fail to find a parameterisation that would fit the MHVSR data at high frequencies as well as the dispersion data. We achieve a compromise where we fit the MHVSR fundamental peak and sacrifice fitting the MHVSR at higher frequencies in preference to the dispersion data. For the Tsawwassen site, agreement with only the general trend of the dispersion data is achieved (the dispersion data is rather complex). At this site we also failed to

obtain a clear MHVSR peak, which we attributed to a weak impedance contrast between glacial sediment and bedrock below occurring at significant depth.

3.6.1. V$_S$ profile interpretation

We can evaluate the success of our V$_S$ profiling from comparison with the closest stratigraphic profiles from Armstrong (1984; Figure 3.1). For sites in the northwest of the Lower Mainland located on uplands Pleistocene sediments (East Vancouver, South Vancouver, Burnaby and Coquitlam; Figure 3.2), we determine a major impedance contrast at 80-110 m depth, with the exception of the Coquitlam East site, where it is determined as deep as 160 m. The nearest available stratigraphic profile to the East Vancouver, South Vancouver and Killarney sites in a similar geological setting (~4 km away; Profile 7 in Armstrong, 1984) shows 115 m of various sediments overlying Tertiary bedrock, which supports our inversion estimates. The Killarney site exists within a small mapped pocket of lowland sediment (Unit 2, Turner et al., 1997) in agreement with our inversion model with a ~20 m layer of low V$_S$ (~200 m/s).

The relatively moderate V$_S$ (500-800 m/s) determined to depths of up to 110 m and 160 m at the two Coquitlam sites on uplands Pleistocene sediment agree with a nearby stratigraphic profile from a cliff south of Port Moody (Profile 21 in Armstrong, 1984) which logged at least 100 m of soft sands, gravels, silts, and tills. The moderate V$_S$ (~600 m/s) and major impedance contrast estimates for both Port Coquitlam sites (90 and 150 m) agree with a nearby borehole stratigraphic profile beneath the Pitt River Bridge (Profile 45, Armstrong, 1984), which logged at least 80 m of sediments over bedrock. Despite being only 1.4 km apart, our V$_S$ profile for the second Port Coquitlam site has a greater depth to a major impedance contrast, and ~40 m of a very soft (V$_S$ ~200 m/s) sediment. This can be attributed to its location slightly further eastward in the Fraser Valley, where lowland gravels and sands are mapped at surface (Figure 3.2).

At the Tsawwassen site, situated on upland Pleistocene glacial deposits at the southern tip of the Lower Mainland (Figure 3.2), we determine a thin (< 10 m) soft layer (V$_S$ ~240 m/s), overlying stiff material (V$_S$ of ~450 m/s) to a depth of around 170 – 200 m. A deep interface here is found by both Britton (1995), who estimates a depth to bedrock of

around 500 m from seismic reflection, and Armstrong (1984; Profile 10), who found a depth to bedrock of 260 m at a nearby borehole stratigraphic profile from Tsawwassen. We suspect the impedance contrast is relatively weak and deep, making it harder to resolve from our dispersion and MHVSR datasets, which is why we failed to observe a clear MHVSR peak. The dispersion curve also seems to show a 'trough' at 3-5 Hz, which could indicate a low velocity zone within the Pleistocene sequence, however the inversion process did not fit this.

Borehole stratigraphic profiles near Abbotsford (Profiles 37 and 38, Armstrong, 1984) show depths to bedrock of ~110 m and 160 m. Our estimate of a major impedance contrast depth of 120-180 m at Abbotsford is in general agreement with this. A nearby stratigraphic cross-section of the Fraser River valley (Profile 48) also establishes a highly variable bedrock depth, changing from 30 m to 90 m over a lateral extent of 300 m.

At our Colwood delta site on southern Vancouver Island, we determine a thin ~7 m layer of V_S of ~400 m/s, overlying ~500 m/s to a major impedance contrast at 60 m depth. The top layer agrees with the V_S estimates of the Colwood delta sand and gravel deposits (~330 m/s, Monahan and Levson, 2001), whereas the higher V_S layer agrees with V_S of Pleistocene deposits (~500 m/s; Monahan and Levson 1997). Monahan and Levson (2001) observed V_{Save} of 330 ± 55 m/s at depths up to 11 m at two sites inside the delta, and south of the Esquimalt Lagoon near our site, the delta sediments overlie Pleistocene deposits of over 50 m thickness (Monahan and Levson, 2000). Our V_S profile matches well with these previous observations.

The site in Hope is located in the Fraser River valley, at a location where we expect thick fluvial sediments (Monger & Lear, 1989). Our V_S profile shows three distinct layers, although the match with the MHVSR data at high frequencies is not ideal, so the uppermost V_S layer is uncertain. We determine slightly lower V_S (~400 m/s) for the upper ~15 m which are likely the Fraser River sediments. Slightly higher V_S (~600 m/s) are likely Pleistocene sediments up to a possible Tertiary bedrock interface at 80 m depth. The significant impedance contrast (potential bedrock depth) estimate for Surrey is 50 - 60 m. The site is located on uplands till (Figure 3.2). We determine a high V_S of ~700

m/s between 10-60 m depth that likely corresponds to very stiff Pleistocene sediments. A nearby borehole stratigraphic profile (Profile 14, Armstrong 1984) logged a depth to bedrock of ~360 m. This is the only case in which there was a large disparity between our estimate of a significant impedance contrast (base of Pleistocene or bedrock depth) and the known bedrock depth. The relatively high frequency of our MHVSR (> 2 Hz) and dispersion (> 5 Hz) data suggests we can only resolve to the depth of the Pleistocene sediments. However, a significant impedance contrast must occur at ~60-m depth related to the observed moderate amplitude MHVSR peak frequency at 3-4 Hz. This is a prime example of how variable the bedrock depth may be below the Surrey uplands and site-specific measurements are required.

3.6.2. Site classification comparison

Table 3.2 summarizes our site-specific *in situ* site classification determination for 13 investigated sites. $V_{S30,}$ is calculated from the minimum misfit inverted V_S depth profile and associated site classification (Table 1.1) is assigned according to Canadian building and bridge codes. Depth to a major impedance contrast is the depth to the top of the elastic half-space in our V_S profile (likely Tertiary bedrock depth in most cases as discussed further below); peak frequency is obtained from the observed MHVSRs. Site classes for all 13 sites vary between class D and C, which represent stiff soil and dense soil/soft rock respectively.

Table 3.2 also compares our site class results to those of previous studies: (1) an interpolated map from ~500 Fraser delta V_S profiles (Hunter and Christian 2001), (2) a combination map of the Fraser delta data with mapped Quaternary geology (Monahan 2005), and (3) a map of topographic slope proxy-V_{S30} estimates (Allen and Wald 2009). Although these previous classifications are largely from interpolated maps and not site-specific measurements, they offer a direct comparison to evaluate our results. In some cases due to the low resolution of the previous studies and interpolation between map points, the mapped classification of our measured sites is ambiguous, and could arguably belong to either of two classes (e.g., C or D, and D or E). Our site-specific V_{S30} classifications agree with the global USGS V_{S30}-proxy map (Allen and Wald 2009) for 11

sites; for the remaining 2 sites, we model lower amplification potential (class C compared to D). At East Vancouver, Killarney and South Vancouver sites, we model a higher amplification hazard (lower site class) than that interpolated from previous V_S measurements (Hunter and Christian 2001), which for Killarney is two classes higher. This can be attributed to the interpolation of V_{S30} values towards the north in the Hunter and Christian (2001) map, as they did not sample the small pocket of lowland sediment that our Killarney site sits on (Turner et al., 1997). Our results generally show a good agreement with Monahan (2005); we obtain the same site class in 8 of 10 cases. In Port Coquitland South, we determine a site class of D compared to Monahan's mapped class E, whereas at Port Coquitlam North we determine a lower hazard site class (C compared to D/E). Monahan's V_{S30} classification mapping is assigned from V_S measurements in similar mapped Quaternary geologic units in the region (V_S has not been measured at the site of interest).

Table 3.2. Site classification estimates from our joint inversion results compared to previous classification estimates for our 13 sites (sorted by site class).

Location	Depth to major impedance contrast (m)	V_{S30} (m/s)	f_{peak} (Hz)	Site class			
				Our model	Hunter & Christian (2001)	Monahan (2005)	Allen & Wald (2009)
Burnaby	~ 80	480	3.3	C		C	C
Colwood	~ 60	480	2.5	C			C
Coquitlam East	~ 160	630	1.4	C		C	C/D
East Vancouver	~ 110	490	1.7	C	B	C	C/D
Hope	~ 80	450	1.3	C			D
Port Coquitlam North	~ 90	500	1.9	C		D/E	D
South Vancouver	~ 110	480	1.2	C	B	C	C
Surrey	50 - 60	590	4.0	C		C	C
Tsawwassen	170 - 200	370	-	C	C/D	C	C
Coquitlam West	~ 110	350	1.3	C/D		C	C/D
Abbotsford	120 - 180	270	1.0	D			D
Killarney	~ 80	300	2.0	D	B	C/D	C/D
Port Coquitlam South	~ 150	190	1.0	D		E	D

3.7. Discussion and Conclusions

We successfully retrieve V_S profiles and important site response parameters (V_{S30}, peak frequency, depths of significant impedance contrasts) at all measured sites. We show that non-uniqueness in the inversion process can be effectively reduced using the combination of joint inversion of unique datasets (MHVSR and dispersion) and *a priori* data from existing geological and stratigraphic data, even when sparse. Our use of passive seismic methods to rapidly obtain V_S profiles across Greater Vancouver reinforces how these non-invasive methods offer an attractive alternative to traditional V_S profiling methods, due to the speed of acquisition and processing, and applicability to urban environments. The quality of our results is evidenced by the good agreement with existing stratigraphic profiles, where available.

In this study, we determine V_{S30} from site-specific measurement of passive seismic (microtremor) recordings. We are confident that our V_S-measured site classifications offer a more accurate representation of site amplification for our specific locations when compared to previous non-site-specific classifications and interpolations. However, in general, our V_{S30} estimates do compare well to these alternative methods. It is important to note that this study does not invalidate proxy-based V_{S30} methods, which are advantageous for regional mapping due to their ease and speed. In future studies an integration of various proxy-based and V_S measurement datasets could be achieved to obtain an extensive regional V_{S30} map that is also constrained by dense site-specific V_{S30} measurements, similar to that created for California by Thompson et al. (2014).

Our V_S profiling at 13 school sites contributes to publically available V_S measurements in the region, which will in turn support regional-scale earthquake site amplification (microzonation) mapping. The success of this study provides confidence for future passive seismic site assessment, and serves as the basis for an initiated 5-year seismic microzonation effort in the region. V_S information at many more survey locations is required across southwest BC to improve our knowledge of lateral heterogeneity and increase the resolution of the mapping. By combining passive/active-source seismic methods with remote-sensing proxy techniques (e.g. geology, topographic slope), we can

reach a compromise between the speed of proxy methods with the accuracy of site-specific measurements. Additional future work could include joint inversion of the datasets with more sophisticated forward algorithms (e.g., MHVSR resulting from diffuse waves) and quantification of model parameter uncertainties at each site using the variability of the inversion results.

3.8. Acknowledgements

3.9. References

Aki, K. (1957). Space and time spectra of stationary stochastic waves, with special reference to microtremors. *Bulletin of the Earthquake Research Institute, University of Toronto*, *35*, 415–456.

Allen, T. I., & Wald, D. J. (2009). On the Use of High-Resolution Topographic Data as a Proxy for Seismic Site Conditions (VS30). *Bulletin of the Seismological Society of America*, *99*(2A), 935–943. http://doi.org/10.1785/0120080255

Arai, H., & Tokimatsu, K. (2004). S-Wave Velocity Profiling by Inversion of Microtremor H/V Spectrum. *Bulletin of the Seismological Society of America*, *94*(1), 53–63. http://doi.org/10.1785/0120030028

Arai, H., & Tokimatsu, K. (2005). S-wave velocity profiling by joint inversion of microtremor dispersion curve and horizontal-to-vertical (H/V) spectrum. *Bulletin of the Seismological Society of America*, *95*(5), 1766–1778. http://doi.org/10.1785/0120040243

Armstrong, J. E. (1984). Environmental and engineering applications of the surficial

geology of the Fraser Lowland, British Columbia. *Geological Survey of Canada Paper*, *83–23*.

Asten, M. W., & Henstridge, J. (1984). Array estimators and the use of microseisms for reconnaissance of sedimentary basins. *Geophysics*, *49*(11), 1828–1837.

Bettig, B., Bard, P. Y., Scherbaum, F., Riepl, J., Cotton, F., Cornou, C., & Hatzfeld, D. (2001). Analysis of dense array noise measurements using the modified spatial auto-correlation method (SPAC): application to the Grenoble area. *Bollettino Di Geofisica Teorica Ed Applicata*, *42*(3–4), 281–304.

Bonnefoy-Claudet, S., Cornou, C., Bard, P. Y., Cotton, F., Moczo, P., Kristek, J., & Fäh, D. (2006). H/V ratio: A tool for site effects evaluation. Results from 1-D noise simulations. *Geophysical Journal International*, *167*(2), 827–837. http://doi.org/10.1111/j.1365-246X.2006.03154.x

Bonnefoy-Claudet, S., Kohler, A., Cornou, C., Wathelet, M., & Bard, P.-Y. (2008). Effects of Love Waves on Microtremor H/V Ratio. *Bulletin of the Seismological Society of America*, *98*(1), 288–300. http://doi.org/10.1785/0120070063

Boore, D. M., Thompson, E. M., & Cadet, H. (2011). Regional correlations of V s30 and velocities averaged over depths less than and greater than 30 meters. *Bulletin of the Seismological Society of America*, *101*(6), 3046–3059. http://doi.org/10.1785/0120110071

Borcherdt, R. D. (1994). Estimates of Site- Dependent Response Spectra for Design (Methodology and Justification). *Earthquake Spectra*. http://doi.org/10.1193/1.1585791

Britton, J. R., Harris, J. B., Hunter, J. A., & Luternauer, J. L. (1995). The bedrock surface beneath the Fraser River delta in British Columbia based on seismic measurements. *Current Research*, *83–89*.

Capon, J. (1969). High-resolution frequency-wavenumber spectrum analysis. *Proceedings of the IEEE*, *57*(8), 1408–1418. http://doi.org/10.1109/PROC.1969.7278

Carniel, R., Barazza, F., & Pascolo, P. (2006). Improvement of Nakamura technique by singular spectrum analysis. *Soil Dynamics and Earthquake Engineering*, *26*(1), 55–63. http://doi.org/10.1016/j.soildyn.2005.08.005

Cassidy, J. F., & Rogers, G. C. (2004). Variation in ground shaking on the Fraser River delta (Greater Vancouver , Canada) from analysis of moderate earthquakes. In *13th World Conference on Earthquake Engineering* (p. 7).

Dal Moro, G. (2014). *Surface wave analysis for near surface applications* (1st Edition). Elsevier.

Delgado, J., López Casado, C., Giner, J., Estévez, a., Cuenca, a., & Molina, S. (2000). Microtremors as a Geophysical Exploration Tool: Applications and Limitations. *Pure and Applied Geophysics*, *157*(9), 1445–1462. http://doi.org/10.1007/PL00001128

Google Maps. (2017). Map of Ecole Alpha Secondary, Burnaby, BC. *Retrieved from https://goo.gl/maps/WMniaPGXPg82*.

Haskell, N. A. (1960). Crustal reflection of plane SH waves. *Journal of Geophysical Research*, *65*(12), 4147–4150. http://doi.org/10.1029/JZ065i012p04147

Herrmann, R. (1987). Computer programs in seismology. *St Louis University, St. Louis, Missouri*.

Hunter, J. A., & Christian, H. A. (2001). Use of Shear Wave Velocities to Estimate Thick Soil Amplification Effects in the Fraser River Delta, British Columbia. *Symposium on the Application of Geophysics to Engineering and Environmental Problems 2001*, (March), SSI1-SSI1. http://doi.org/10.4133/1.2922943

Hunter, J. A., Dallimore, S., & Christian, H. (1997). Borehole measurements of shear wave velocity discontinuities in Quaternary sediments, Fraser River delta, British Columbia. *Current Research 1997-A, Geological Survey of Canada*.

Hunter, J. A., Douma, M., Burns, R. A., Good, R. L., Pullan, S. E., Harris, J. B., Luternauer, J. L., & Best, M. E. (1998). Testing and application of near-surface geophysical techniques for earthquake hazards studies, Fraser River delta, British Columbia. *Bulletin of the Geological Survey of Canada*, (525), 123–145.

Konno, K., & Ohmachi, T. (1998). Ground-motion characteristics estimated from spectral ratio between horizontal and vertical components of microtremor. *Bulletin of the Seismological Society of America*, *88*(1), 228–241.

Kramer, S. L. (1996). *Geotechnical Earthquake Engineering*. *Geotechnical earthquake engineering* (Vol. 80). Upper Saddle River, NJ: Prentice-Hall.

Lacoss, R., Kelly, E., & Toksöz, M. (1969). Estimation of seismic noise structure using arrays. *Geophysics*, *34*(1), 21–38.

Lomax, A., & Snieder, R. (1994). Finding sets of acceptable solutions with a genetic algorithm with application to surface wave group dispersion in Europe. *Geophysical Research Letters*, *21*(24), 2617–2620. http://doi.org/10.1029/94GL02635

Molnar, S., Crow, H., Ventura, C., Finn, W., & Stokes, T. (2014). Regional seismic hazard assessment for small urban centers in Western Canada. *In Proceedings of the 10th National Conference in Earthquake Engineering*.

Molnar, S., Dosso, S. E., & Cassidy, J. F. (2010). Bayesian inversion of microtremor array dispersion data in southwestern British Columbia. *Geophysical Journal International*, *183*(2), 923–940. http://doi.org/10.1111/j.1365-246X.2010.04761.x

Molnar, S., Dosso, S. E., & Cassidy, J. F. (2013). Uncertainty of linear earthquake site amplification via Bayesian inversion of surface seismic data. *Geophysics*, *78*(3), WB37-WB48.

Monahan, P. A. (2005). Soil hazard map of the lower mainland of British Columbia for assessing the earthquake hazard due to lateral ground shaking. *9th Canadian Conference on Earthquake Engineering*.

Monahan, P. A., & Levson, V. (2000a). Quaternary geological map of Greater Victoria. *Geoscience Map 2000-2*, *12*(1974), 2000.

Monahan, P. A., & Levson, V. (2001). Development of a shear-wave velocity model of the near-surface deposits of southwestern British Columbia, Canada. *Fourth International Conference on Recent Advances in Geotechnical Eathquake Engineering and Soil Dynamics*, 1–12.

Monahan, P. A., & Levson, V. M. (2000b). Quaternary Geological Map of Greater Victoria, British Columbia. *Geological Survey, Ministry of Energy and Mines, Victoria, B.C., Geoscience Map 2000*, *2*.

Monahan, P. A., Luternauer, J. L., & Barrie, J. V. (1993). A delta plain sheet sand in the Fraser River delta, British Columbia, Canada. *Quaternary International*, *20*(C), 27–38. http://doi.org/10.1016/1040-6182(93)90034-D

Monger, J. W. H., & Lear, S. (1989). Geology, Hope, British Columbia. *Geological Survey of Canada, Preliminary Map 41-1989*. http://doi.org/10.4095/127735

Nakamura, Y. (1989). A method for dynamic characteristics estimation of subsurface using microtremor on the ground surface. *Railway Technical Research Institute, Quarterly Reports*, *30*(1).

Nogoshi, M., & Igarashi, T. (1971). On the amplitude characteristics of microtremor (part 2). *J. Seismol. Soc. Japan*, *24.1*, 26–40.

Park, C. B., Miller, R. D., & Xia, J. (1999). Multichannel analysis of surface waves (MASW). *Geophysics*, *64*(3), 800–808. http://doi.org/10.1190/1.1444590

Park, S., & Elrick, S. (1998). Predictions of shear-wave velocities in southern California using surface geology. *Bulletin of the Seismological Society of America*, *88*(3), 677–685.

Parolai, S., Picozzi, M., Richwalski, S. M., & Milkereit, C. (2005). Joint inversion of phase velocity dispersion and H/V ratio curves from seismic noise recordings using a genetic algorithm, considering higher modes. *Geophysical Research Letters*, *32*(1), L01303. http://doi.org/10.1029/2004GL021115

Rothman, D. (1985). Large near-surface anomalies, seismic reflection data, and simulated annealing. *Doctoral Dissertation, Stanford University*.

Sambridge, M., L.R., J., E.L., M., W.T., V., & E., T. (1999). Geophysical inversion with a neighbourhood algorithm-II. Appraising the ensemble. *Geophysical Journal International*, *138*(3), 727–746. http://doi.org/10.1046/j.1365-246x.1999.00900.x

Scherbaum, F., Hinzen, K.-G., & Ohrnberger, M. (2003). Determination of shallow shear wave velocity profiles in the Cologne, Germany area using ambient vibrations. *Geophysical Journal International*, *152*(3), 597–612. http://doi.org/10.1046/j.1365-246X.2003.01856.x

Stokoe, K. H., Nazarian, S., Rix, G. J., Sanchez-Salinero, I., Sheu, J.-C., & Mok, Y.-J. (1988). In situ seismic testing of hard-to-sample soils by surface wave method. In *Geotechnical Special Publication*.

Tarantola, A. (1987). *Inverse problem theory: Methods for Data Fitting and Model Parameter Estimation*. Elsevier.

Thompson, E. M., Wald, D. J., & Worden, C. B. (2014). A VS30 Map for California with geologic and topographic constraints. *Bulletin of the Seismological Society of America*, *104*(5), 2313–2321. http://doi.org/10.1785/0120130312

Tinsley, J., & Fumal, T. (1985). Mapping Quaternary sedimentary deposits for areal variations in shaking response. *Valuating Earthquake Hazards in the Los Angeles Region—An Earth Science Perspective, 1360, 101-126.*

Tokimatsu, K. (1997). Geotechnical site characterisation using surface waves. *Earthquake Geotechnical Engineering*, 1333–1368.

Turner, R. J. W., Clague, J. J., Groulx, B. J., & Journeay, J. M. (1997). GeoMap Vancouver, Geological Map of the Vancouver Metropolitan Area. *Geological Survey of Canada Open File 3511.*

Ventura, C., Turek, M., Johansen, K., Kaya, Y., Yao, F., & Southby, B. (2017). British Columbia earthquake early warning system. *Proceedings 16th World Conference on Earthquake Engineering, Santiago, Chile, Paper 4662*.

Wair, B. R., Dejong, J. T., & Shantz, T. (2012). Guidelines for Estimation of Shear Wave Velocity Profiles. *Pacific Earthquake Engineering*, *8*(December), 68.

Wald, D. J., & Allen, T. I. (2007). Topographic slope as a proxy for seismic site conditions and amplification. *Bulletin of the Seismological Society of America*. http://doi.org/10.1785/0120060267

Wathelet, M. (2005). Array recordings of ambient vibrations: surface-wave inversion. *PhD Thesis, Universit´e de Li`ege, Belgium.*

Wathelet, M. (2008). An improved neighborhood algorithm: Parameter conditions and dynamic scaling. *Geophysical Research Letters*, *35*(9), L09301. http://doi.org/10.1029/2008GL033256

Wathelet, M. (2017). Geopsy Version 2.10.1: Geophysical Signal Database for Noise Array Processing. *Software, LGIT, Grenoble, France*.

Wathelet, M., Jongmans, D., Ohrnberger, M., & Bonnefoy-Claudet, S. (2008). Array performances for ambient vibrations on a shallow structure and consequences over Vs inversion. *Journal of Seismology*, *12*(1), 1–19. http://doi.org/10.1007/s10950-007-9067-x

Wiggins, R. A. (1969). Monte Carlo inversion of body-wave observations. *Journal of Geophysical Research*, *74*(12), 3171–3181. http://doi.org/10.1029/JB074i012p03171

Wightman, W. E.; Jalinoos, F.; Sirles, P.; Hanna, K. (2003). Application of Geophysical

Methods to Highway Related Problems. *Federal Highway Administration, Central Federal Lands Highway Division, Lakewood, CO, Publication No. FHWA-IF-04-021*, 742.

Zhao, D., & Li, V. (2010). Comparison Of FK And Spac Methods In Determining Dispersion Curves From Passive Surface Wave. *23rd EEGS Symposium on the Application of Geophysics to Engineering and Environmental Problems*.

Chapter 4

4. Conclusions

4.1. Summary

In Chapter 2, we used strong-motion recordings of the 2015 **M** 4.7 Vancouver Island earthquake to re-evaluate local variations in the ground motion in southwest BC, including how these motions relate to site effects. Strong-motion recordings were obtained and processed from the BCSIMS strong-motion IA network from 56 strong-motion stations operating within 100 km of the earthquake epicentre. We found lower amplification (factor of 1-3) at most sites in Vancouver, which we attributed to the presence of relatively stiff Pleistocene post-glacial sediments here. We found higher amplification (factor of 3-5) on the Holocene Fraser River delta sediments, and noted that the strongest amplification occurs at sites on the northern edge of the delta as observed in previous earthquakes. In a few cases, amplification in Vancouver is similar to softer Fraser River delta sites. The observed decreasing site amplification from soft delta sediments to stiffer Pleistocene sediments generally agrees with current microzonation maps based on Quaternary geology. However these maps do not capture observed local discrepancies in site amplification, including the delta edge amplification and higher amplification at a few Vancouver sites. We conclude that current microzonation maps do not accurately predict observed earthquake shaking, and that higher density site-specific V_S measurements (accurate site classifications) are required.

The M 4.7 earthquake also produced the first borehole recordings obtained at depth in BC, which provide the first opportunity to examine the variation of earthquake shaking amplitude with depth in the Lower Mainland. We observe recorded motions that increase towards the surface and are of similar or higher amplitude than at nearby surface stations. Amplification between top and bottom sensors is a consistent factor of 7-8 in all three arrays over a similar 40-45 m depth interval of Fraser delta sediments. Cross-correlation analysis determines shear wave velocity estimates < 350 m/s, which is consistent with delta sediments.

In Chapter 3, we use passive seismic methods to obtain site-specific V_S profiles and important site amplification parameters (V_{S30}, peak frequency, depths of significant impedance contrasts) at 13 sites in southwest BC. At each site, arrays of varying radii and up to 9 three-component sensors recorded simultaneous ambient vibrations. Microtremor HVSRs are computed to obtain peak frequencies, and surface wave array analyses are performed to obtain Rayleigh wave dispersion estimates. Joint inversion of the low-frequency MHVSR and high-frequency dispersion datasets are performed to obtain V_S profiles, resolved over as full a depth interval as possible, for each site. We compare the Vs profiles with nearby stratigraphy to interpret whether known geologic horizons agree with our determined impedance contrasts. Each site's V_S profile is then used to provide the average V_S of the upper 30 m and associating NBCC earthquake site class. For the 13 sites, V_{S30} corresponds to site classifications that vary between class D (stiff soil) and C (dense soil/soft rock). Generally we find a good match between classifications from previous studies and our site classifications.

4.2. Discussion

This thesis contributes to an initiated 5-year seismic microzonation effort in southwest BC. This project aims to improve earthquake site classifications by characterizing the S-wave velocity of local geology in order to more accurately model site amplification potential. The analyses in Chapters 2 and 3 address two important aspects of improving seismic hazard assessment in Greater Vancouver. Chapter 2 involves reassessing general spatial variations in observed earthquake site effects using recent earthquake data, whereas Chapter 3 involves using *in situ* passive seismic measurements to determine earthquake site classification at each site of interest based on site-specific V_S measurements. The success of our passive seismic methods in determining detailed site characterization information provides confidence for future use in regional microzonation mapping.

Chapter 2 describes how observed ground motions are only broadly described by Quaternary geological and current microzonation mapping. This is because site effects are a complex phenomenon, involving the contribution of subsurface properties discussed

in Chapter 1. Chapter 2 highlights the need for improved site classification in southwest BC, which must be both accurate and feasible to perform rapidly over a large area. Chapter 3 is a proof of concept for the use of passive seismic methods to improve earthquake site classification and address the issues raised in Chapter 2. We believe that because of the complexity of site effects, simplistic proxy-based methods (e.g., topographic slope or surficial geology) for estimating site characterization parameters may not be sufficient to predict site amplification. These proxy-based V_{S30} methods do not capture subsurface V_S variations and are subject to large uncertainties. Non-invasive seismic methods are advantageous over invasive borehole techniques due to the large spatial scales needed for microzonation.

Passive-source methods are preferred over active-source methods as they include a larger frequency bandwidth, allowing a sampling of a larger range of depths, and they are more applicable to urban applications. The general practice in geophysical V_S profiling is to use both active (high frequencies) and passive (low frequencies) methods to maximise the frequency bandwidth of the dispersion curve (Hunter & Crow, 2012). We find that the joint inversion of two solely passive seismic datasets (MHVSR and SPAC) provides a sufficient bandwidth that can adequately retrieve a site-specific V_{S30} value. It is our opinion that the benefits of active source providing high frequency dispersion data are outweighed by the logistical drawbacks of active acquisition (larger arrays, more disruptive).

Although there is on-going discussion on the applicability of V_{S30} to site classification (see Chapter 1), all alternative parameters (e.g., full V_S profile, site period, V_{S10}) are obtainable by a non-invasive passive-seismic (surface wave and ambient vibration) methodology, as demonstrated in this study. Measurement of f_{peak} from a MHVSR only requires a single three-component sensor, so acquisition is even faster than array-based dispersion methods. We conclude that passive seismic analysis methods (both single station MHVSR and surface wave array methods) are an attractive method for accurate regional-scale mapping of seismic hazard or microzonation, with numerous advantages over traditional methods, especially in urban environments.

4.3. Future Work

The analysis of site effects from earthquake data is an important part of seismic hazard assessment that must be repeated on an event specific basis, as different earthquakes generate different frequency content that result in resonance at specific sediment thicknesses. Evaluation of the spatial variation of ground motions also offers a way to test amplification mapping metrics in Greater Vancouver, so future work must involve similar analysis using new earthquake data.

Although V_S is the principal parameter used currently in earthquake site classification, many recent seismic microzonation maps consist of predominant period distribution, using rapidly acquired passive HVSR measurements (e.g. Tuladhar et al., 2004; Fnais et al., 2010; Büyüksaraç et al., 2013; Navarro et al., 2014). Hassani and Atkinson (2016) recently demonstrated that V_{S30} can be effectively proxied from earthquake HVSRs in the calculation of GMPEs. GMPE studies are being developed using just f_{peak} and sediment stiffness to capture site amplification rather than V_{S30} (Braganza et al., 2016). It is possible that more focus will be placed in future on potential use of f_{peak} and future surveys should take this into account.

The site classification assessments in Chapter 3 can be used for detailed seismic hazard analysis, such as using geotechnical simulation software to obtain site response and amplification spectra. Ground motion modelled from accurate site amplification estimates can then be combined with building vulnerability evaluations for seismic risk (loss) and damage assessment. However the data in Chapter 3 are limited by sample size for regional microzonation mapping applications; passive seismic data were only collected at 13 sites. Future measured V_S profiling at many more survey locations across southwest BC is required to improve our knowledge of lateral heterogeneity, increase the resolution of the mapping, and add to the database of knowledge of regional V_S for possible future modelling using proxy methods. High-resolution mapping also allows the modelling of 3D effects (e.g. basin effects).

A major disadvantage of our results is the lack of quantification of uncertainty, which could arise form errors in the dispersion curves (e.g., manual picking), as well as from the

non-uniqueness of the solution. This could be quantified in future studies by assessing the variability of the lowest misfit models, or by using a more advanced inversion algorithm. For example, Bergamo et al. (2011) used a Monte Carlo inversion algorithm to invert surface wave data based on a multimodal misfit function that provides estimates of uncertainty related to solution non-uniqueness.

A future integration of alternative data sets is possible: Havenith et al. (2007) performed microzonation of the Basel region in Switzerland by integrating array measurements, SASW, reflection, and borehole data, and noted the benefit from the different depth sensitivities of the individual methods. In Chapter 3 we also discussed the possibility of combining seismic methods with remote-sensing proxy techniques (e.g. geology, topographic slope), as this offers a compromise between the speed of proxy methods with the accuracy of site-specific measurements. For example Thompson et al. (2014) were successful in the integration of topographic data with geology and site-specific measurements for California. However V_{S30} uncertainty was found to be significantly reduced in areas of denser site-specific measurement. Similarly Scott et al (2006) performed a fast and economic 13 km survey in Las Vegas using 49 Rayleigh wave dispersion measurements, and extrapolated their model using geological and soil maps with moderate success. They found that in areas of sparse measurements accuracy of V_{S30} estimates was reduced by around 20%. These studies indicate that site-specific seismic methods are still the primary dataset for any such study.

4.4.   References

Bergamo, P., Comina, C., Foti, S., & Maraschini, M. (2011). Seismic characterization of shallow bedrock sites with multimodal Monte Carlo inversion of surface wave data. *Soil Dynamics and Earthquake Engineering*, *31*(3), 530–534. http://doi.org/10.1016/j.soildyn.2010.10.006

Braganza, S., Atkinson, G. M., Ghofrani, H., Hassani, B., Chouinard, L., Rosset, P., Motazedian, D., & Hunter, J. (2016). Modeling Site Amplification in Eastern Canada on a Regional Scale. *Seismological Research Letters*, *88*(3).

Büyüksaraç, A., Bektaş, Ö., Yılmaz, H., & Arısoy, M. Ö. (2013). Preliminary seismic

microzonation of Sivas city (Turkey) using microtremor and refraction microtremor (ReMi) measurements. *Journal of Seismology*, *17*(2), 425–435. http://doi.org/10.1007/s10950-012-9328-1

Fnais, M. S., Abdelrahman, K., & Al-Amri, A. M. (2010). Microtremor measurements in Yanbu city of Western Saudi Arabia: A tool for seismic microzonation. *Journal of King Saud University - Science*, *22*(2), 97–110. http://doi.org/10.1016/j.jksus.2010.02.006

Hassani, B., & Atkinson, G. M. (2016). Applicability of the NGA- West2 Site- Effects Model for Central and Eastern North America. *Bulletin of the Seismological Society of America*, *106*(3), 1331–1341. http://doi.org/10.1785/0120150321

Havenith, H.-B., Fäh, D., Polom, U., Roullé, A., S., T., & T., C. (2007). S-wave velocity measurements applied to the seismic microzonation of Basel, Upper Rhine Graben. *Geophysical Journal International*, *170*(1), 346–358. http://doi.org/10.1111/j.1365-246X.2007.03422.x

Hunter, J. A., & Crow, H. L. (2012). Shear wave velocity measurement guidelines for canadian seismic site characterization in soil and rock. *Geological Survey of Canada*, *Open File*(7078), 227. http://doi.org/10.4095/291753

Navarro, M., García-Jerez, A., Alcalá, F. J., Vidal, F., & Enomoto, T. (2014). Local site effect microzonation of Lorca town (SE Spain). *Bulletin of Earthquake Engineering*, *12*(5), 1933–1959. http://doi.org/10.1007/s10518-013-9491-y

Thompson, E. M., Wald, D. J., & Worden, C. B. (2014). A VS30 Map for California with geologic and topographic constraints. *Bulletin of the Seismological Society of America*, *104*(5), 2313–2321. http://doi.org/10.1785/0120130312

Tuladhar, R., Yamazaki, F., Warnitchai, P., & Saita, J. (2004). Seismic microzonation of the greater Bangkok area using microtremor observations. *Earthquake Engineering & Structural Dynamics*, *33*(2), 211–225. http://doi.org/10.1002/eqe.345

Appendices

Figure A1 displays the time-averaged MHVSR obtained for Tsawwassen. The MHVSR is rejected for inversion due to lack of a clear peak.
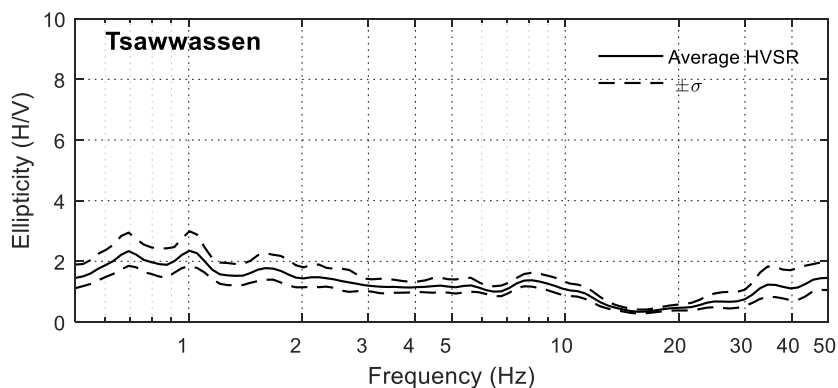

Figure A1. Time-averaged MHVSR for Tsawwassen shown with one standard deviation.

Figure A2 shows Phase velocity histogram from MSPAC analysis at East Vancouver, which was rejected for inversion due to lack of a clear dispersion trend.
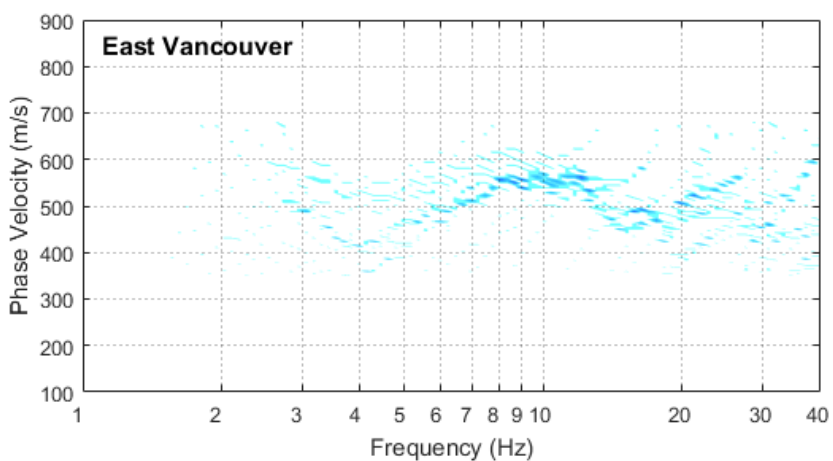

Figure A2. MSPAC histogram stacked cumulatively for East Vancouver arrays shown in blue, where darker shading indicates higher histogram count.

Figure A3 shows the phase velocity histogram from MSPAC analysis at Killarney, which was rejected for inversion due to lack of a clear dispersion trend.
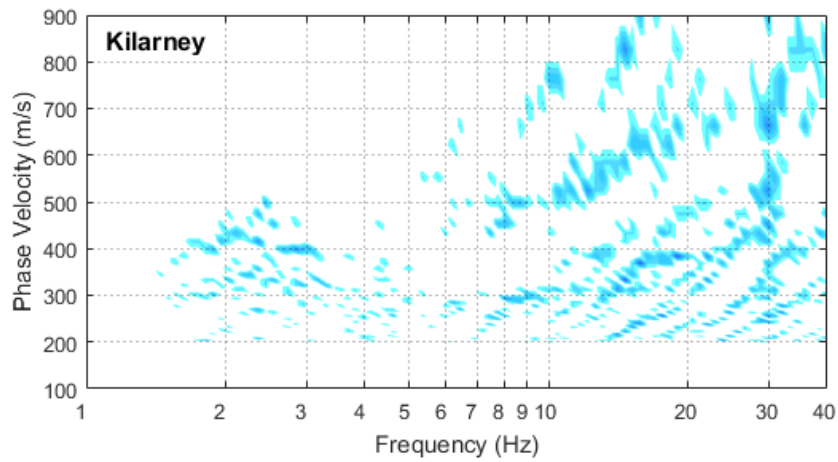

Figure A3. MSPAC histogram stacked cumulatively for Killarney arrays shown in blue, where darker shading indicates higher histogram count.

Curriculum Vitae

Name:	Frederick Andrew Jackson

Post-secondary Education and Degrees:
- University of Leeds (Leeds, England)
  2011-2015 BSc
- Western University (London, Ontario, Canada)
  2015-2017 MSc

Honours and Awards:
- Catastrophe Indices and Quantification Inc. (CatIQ) Canadian Catastrophe Conference (C4), Student Delegate Award, 2017
- Seismological Society of America (SSA) Annual Meeting, 2017 International Travel Grant
- School of Earth and Environment 2011 Attainment Prize

Related Work Experience:
- Teaching Assistant at Western University
  2011-2015
- Visiting Scholar at United States Geological Survey
  May-June 2017

Publications:

Refereed Publications

F. Jackson, S. Molnar, H. Ghofrani, G. M. Atkinson, J. F. Cassidy, and K. Assatourians. (2017). Ground Motions of the December 2015 M 4.7 Vancouver Island Earthquake: Attenuation and Site Response. Bulletin of the Seismological Society of America, accepted.

Refereed Conference Proceedings

F. Jackson, S. Molnar. (2017). The Role of Non-Invasive Ambient Noise Analysis to Improve Seismic Microzonation Mapping in Vancouver, British Columbia, Canada. In Proceedings of 3rd International Conference on Performance-based Design in Earthquake Geotechnical Engineering (PBD-III), Vancouver, BC, July 16-19 2017, Paper 474.

Conference presentations with published abstract

F. Jackson, S. Molnar. (2017). The Role of Non-Invasive Ambient Noise Analysis to Improve Seismic Microzonation Mapping in Vancouver, British Columbia, Canada., Seismological Society of America annual meeting, Denver, Colorado, April 18-20 2017, Poster.

F. Jackson, S. Molnar (2017). The Role of Non-invasive Ambient Noise Analysis in Improving Seismic Microzonation Mapping in Vancouver, British Columbia, Canada. CatIQ's Canadian Catastrophe Conference C4, Toronto, Ontario, February 1-3 2017, Oral and poster.

S. Molnar, J.F. Cassidy, F. Jackson, C. Brillon. (2016). Revisiting Earthquake Site Response in Vancouver, Canada. Seismological Society of America annual meeting, Reno, Nevada, April 20-22 2016, Poster.